Asp1 bi-functional activity modulates spindle function via controlling cellular inositol pyrophosphate levels in *Schizosaccharomyces pombe*

running title: Vip1 pyrophosphatase

Marina Pascual-Ortiz[1], Adolfo Saiardi[2], Eva Walla[1], Visnja Jakopec[1], Natascha A. Künzel[1], Ingrid Span[3], Anand Vangala[1], and Ursula Fleig[1]#.

[1]Eukaryotische Mikrobiologie, Institut für funktionelle Genomforschung der Mikroorganismen, Heinrich-Heine-Universität, 40225 Düsseldorf, Germany

[2]Medical Research Council Laboratory for Molecular Cell Biology, University College London, London WC1E 6BT, UK.

[3]Institut für Physikalische Biologie, Heinrich-Heine-Universität, 40225 Düsseldorf, Germany

Word count: Material and Methods: 1135

Introduction, Results and Discussion: 4987

#Corresponding author email: fleigu@hhu.de

Abstract

The generation of two daughter cells with the same genetic information requires error-free chromosome segregation during mitosis. Chromosome transmission fidelity is dependent on spindle structure/function which requires Asp1 in the fission yeast *Schizosaccharomyces pombe.* Asp1 belongs to the PPIP5Ks/Vip1 family which generates high energy inositol pyrophosphate (IPP) molecules. Here we show that Asp1 is a bi-functional enzyme *in vivo*: Asp1 kinase generates specific IPPs which are the substrates of the Asp1 pyrophosphatase. Intracellular levels of these IPPs directly correlate with microtubule stability: pyrophosphatase loss-of-function mutants raised Asp1-made IPP levels twofold thus increasing microtubule stability while overexpression of the pyrophosphatase decreased microtubule stability. Absence of Asp1-generated IPPs resulted in an aberrant increased spindle association of the *S. pombe* kinesin-5 family member Cut7 which led to spindle collapse. Thus, chromosome transmission is controlled via intracellular IPP levels. Intriguingly, identification of the mitochondria-associated Met10 protein as the first pyrophosphatase inhibitor revealed that IPPs also regulate mitochondrial distribution.

Introduction

Inositol pyrophosphates (IPPs) are signaling molecules present in all eukaryotes and are synthesized by the two enzyme families IP6Ks Kcs1 and PPIP5Ks/Vip1 (1-3). Numerous cellular processes are regulated by these high energy molecules including the activation of innate immune response in mammals and plants, insulin signaling, telomere length maintenance and cell death (4-8). IPP generating enzymes control cell morphogenesis in fungi including that of human fungal pathogens (9-11). In the fission yeast *S. pombe* the PPIP5Ks/Vip1 family member Asp1 is essential for the adaptation to nutrient limitation resulting in the dimorphic switch which allows yeast cells to grow in a substrate-invasive pseudohyphal manner (9). Alteration of the interphase microtubule (MT) cytoskeleton is an important contributor for efficient pseudohyphal growth in *S. pombe* (9) and Asp1 is needed for stability of interphase MTs (10). Assembly and function of the mitotic spindle also relies on Asp1: *S. pombe* cells expressing specific *asp1* variants show aberrant bipolar spindle formation due to altered MT dynamics and spindle forces plus defects at the kinetochore-microtubule interface leading to chromosome missegregation (12).

Two mechanisms have been described for modulation of biological processes by IPPs: pyrophosphorylation or the reversible binding to a protein (13, 14). IPP protein targets appear to be numerous as more than 150 *S. cerevisiae* proteins were isolated in a screen using inositol polyphosphates/pyrophosphates as bait (15).

The best studied IPPs are the two diphosphoinositol pentakisphosphate isoforms, 1-IP_7 and 5-IP_7, and bis-diphosphoinositoltetrakisphosphate 1,5-IP_8. They are synthesized from inositol hexakisphosphate (named IP_6 in the text) by two classes of enzyme families: IP6Ks/Kcs1 and PPIP5Ks/Vip1. Synthesis of 5-IP_7 is carried out by

the 5-kinase activity of IP6Ks/Kcs1 (16, 17) while PPIP5Ks/Vip1 can add a diphosphate group to position 1 of IP_6 or 5-IP_7 thus generating 1-IP_7 and 1,5-IP_8 (named IP_8 in the text), respectively (1, 2, 18, 19). The physiological *in vivo* substrate(s) of the kinase domain of the PPIP5Ks/Vip1 family has not been easy to define in a number of organisms analyzed to date (1-3). However, HPLC analysis of inositol phosphates in an *S. cerevisiae VIP1* deletion strain suggested that Vip1 kinase activity might be responsible for the generation of IP_8 as has been demonstrated for the PPIP5Ks/Vip1family members in *Cryptococcus neoformans* and *Arabidopsis thaliana* (6, 11, 20). Also in mammalian cells PPIP5K are mainly responsible for IP_8 synthesis since only <2% of the IP_7 pool is synthesized by PPIP5K (21).

Cellular IPP levels can be altered upon extrinsic signals. The jasmonate-mediated wound response of *A. thaliana* led to an increase of IP_8 (6). In *D. discoideum* IPPs are greatly increased during the chemotactic response (22) while in mammalian cells IP_8 levels are elevated upon hyperosmotic stress (3, 23). The mechanism(s) by which the relative abundance of IPPs is regulated is not understood. However, enzymes exist that can dephosphorylate IPPs in a non-specific (24-26) or specific manner (27). Thus down-regulation of such enzymes might contribute to increased cellular IPP pools.

In this context, the C-terminal domains of PPIP5Ks/Vip1 family members are of particular interest. PPIP5Ks/Vip1 proteins have a N-terminal kinase domain and a C-terminal domain with homology to histidine-acid-phosphatases (1). The site signature motif of histidine-acid-phosphatases RHxxR and HD (28) is present in PPIP5Ks/Vip1 family members except for the aspartate next to the second histidine (1). Nevertheless, the C-terminal domain of the *S. pombe* PPIP5Ks/Vip1 member Asp1

86 has pyrophosphatase activity *in vitro* (10), which is inhibited by iron-sulfur clusters
87 and is specific for the hydrolysis of the pyrophosphate at position 1 of the inositol ring
88 (29).

89 In this work, we have dissected the function of the Asp1 kinase and pyrophosphatase
90 domains *in vivo* and found that they control intracellular IP_8 levels and thus the
91 biological processes that require these specific IPPs.
92

Results

The Asp1 kinase domain is responsible for the generation of IP_8 *in vivo*

To analyze the *in vivo* function of the Asp1 kinase domain we measured inositol polyphosphates in a wild-type strain and the two mutant strains *asp1*^{D333A} and *asp1Δ*. The amino acid D333 is a key catalytic residue required for Asp1 kinase activity (2), while the entire *asp1*$^{+}$ gene has been deleted in the *asp1Δ* strain (9).

Inositol polyphosphates had not been assayed in *S. pombe* cells before and thus we first defined the growth conditions needed. *S. pombe* is a natural inositol auxotroph and requires inositol in the media ((30) and our observations). 10 µM inositol was the minimum concentration required for normal cell growth. Thus, cells of the three strains were radiolabeled with [^{3}H]inositol in the presence of 10 µM cold inositol. Next, soluble inositol polyphosphates were extracted, fractions separated by HPLC and quantified by scintillation counting (31). The wild-type strain showed three prominent peaks; the most abundant was IP_6, followed by IP_7 and IP_8 (Fig 1A, for standards profile see Fig S1). In the *asp1*^{D333A} and *asp1Δ* strains, the IP_8 peak was absent and the IP_7 peak increased (Fig 1B and 1C, quantification in 1D). Thus Asp1 kinase has enzymatic function *in vivo* generating IP_8 via the IP_7 substrate. We have shown previously that strains without functional Asp1 kinase have defects in two biological processes: (i) chromosome segregation and (ii) the dimorphic switch (9, 10, 12). We can conclude now that these processes require IP_8.

Asp1 pyrophosphatase activity leads to destabilized MTs and an inability to switch to pseudohyphal invasive growth

To understand the *in vivo* function of the Asp1 C-terminal domain, we assayed the consequences of overexpression of wild-type and mutant variants on MT stability and the dimorphic switch. The mutant Asp1 C-terminal proteins were generated by mutating conserved amino acids of the histidine acid phosphatase signature motifs (Fig 2A, M1 and M2, respectively) (1).

A strain expressing the wild-type Asp1 C-terminal domain (amino acids 365-920, Fig 2A) from the thiamine-repressible *nmt1*$^{+}$ promoter was hypersensitive to the MT poison thiabendazole (TBZ) demonstrating that expression of the wild-type pyrophosphatase domain decreased MT stability (Fig 2B, middle panels) (10). However expression of mutant *asp1*$^{365\text{-}920/H397A}$ (mutation at position H397 in M1 motif, Fig 2A) did not lead to TBZ hypersensitivity (Fig 2B, bottom panels) indicating that Asp1$^{365\text{-}920/H397A}$ was non-functional. Protein expression levels of Asp1$^{365\text{-}920}$ and Asp1$^{365\text{-}920/H397A}$ were comparable (Fig S2).

Similarly, the ability to grow in an invasive pseudohyphal manner was abolished in cells expressing *asp1*$^{365\text{-}920}$. A wild-type strain expressing *asp1*$^{365\text{-}920}$ on a plasmid via the *nmt1*$^{+}$ promoter could not grow invasively (Fig 2C, bottom middle panel). Growth *per se* was not affected in *asp1*$^{365\text{-}920}$ expressing cells (Fig 2C, surface growth). On the other hand, *asp1*$^{365\text{-}920/H397A}$ expressing cells grew invasively in numbers comparable to the control (Fig 2C, bottom right and left panel, respectively; quantification on the right).

To understand the possible effect of *asp1*$^{365\text{-}920}$ *and asp1*$^{365\text{-}920/H397A}$ expression on intracellular IPP levels we measured inositol polyphosphates in strains expressing these variants. As expected the wild-type strain transformed with the vector control showed the three peaks for IP_6, IP_7 and IP_8 (Fig 3A). Expression of *asp1*$^{365\text{-}920}$ massively decreased IP_8 levels and increased IP_7 in comparison to the control (Fig

3B and quantification in 3D). Thus, Asp1$^{365\text{-}920}$ has *in vivo* pyrophosphatase activity and the substrate is IP_8.

The inositol polyphosphate profile of *asp1*$^{365\text{-}920/H397A}$ expressing cells did not decrease IP_8 levels as shown for wild-type pyrophosphatase expression (Fig 3B and C and quantification in 3D), demonstrating that this Asp1 variant was enzymatically inactive *in vivo*. In fact, the HPLC profile of *asp1*$^{365\text{-}920/H397A}$ expressing cells consistently showed higher IP_8 peaks than the control strain (Fig 3D). This result raises the interesting possibility that Asp1$^{365\text{-}920/H397A}$ acts as a "dominant negative" that might titrate away a protein/protein complex required for activation of the wild-type pyrophosphatase.

In summary, the Asp1 C-terminal domain has enzymatic activity *in vivo* using IP_8 as substrate. IP_8 is required for MT stability and the ability to switch to pseudohyphal invasive growth. Thus the Asp1 pyrophosphatase domain negatively regulates these two biological processes (Fig 3E).

Correct spindle formation requires the concerted action of several motor proteins and we have shown previously that ectopic expression of the Asp1 pyrophosphatase domain rescued the temperature-sensitive lethal phenotype of a *cut7-446* strain (12). Cut7 belongs to the kinesin-5 Eg5 family of motor proteins, which localize to the spindle midzone and the spindle poles supporting bipolar spindle assembly (32). We assayed the consequences of *asp1*$^{365\text{-}920}$ expression on mitotic Cut7 localization in a strain endogenously expressing *cut7*$^{+}$*-GFP* (33). Live-cell imaging of short spindles (2-3.5 μm) of a *cut7*$^{+}$*-GFP* strain transformed with a control plasmid, revealed fluorescence mainly at the two spindle poles and the spindle midzone (Fig 4A). Cells expressing *asp1*$^{365\text{-}920}$ had a significantly increased Cut7-GFP spindle midzone signal compared to control cells: quantification of the Cut7-GFP signal at the spindle middle

in relation to the spindle pole signals (Fig 4B) revealed that *asp1*$^{365-920}$ expression led to an abnormal increase of Cut7-GFP fluorescence on the spindle (Fig 4C).

We had shown previously that *asp1*^{D333A} mitotic cells showed spindle breakage of short spindles prior to sister chromatid separation (12). Spindle collapse was also observed in *cut7*$^{+}$*-GFP* cells expressing plasmid-encoded *asp1*$^{365-920}$ (Fig 4D). 30 % of such analyzed cells showed short spindles (<4.5 μm) that collapsed between one to three times during our analysis (Fig 4D, Suppl. Movie S1). Interestingly, *asp1*$^{365-920}$ expressing cells with breaking spindles showed significantly higher Cut7-GFP spindle midzone fluorescence than cells with non-breaking spindles (Fig 4E) suggesting that spindle collapse might be mediated by abnormally high amounts of Cut7 on the spindle.

Cut7-GFP signal intensity was also assayed in an *asp1*^{D333A} background. Again we found that in the absence of Asp1 generated IP_8, Cut7-GFP spindle fluorescence was increased significantly (Fig 4F).

The human Eg5 kinesin-5 member is up-regulated in many types of cancer, a feature that correlates with poor prognosis (34). *S. pombe* cells without functional Asp1 kinase have defects in bipolar spindle formation and increased chromosome missegregation (12). As aberrant expression of human Eg5 results in polyploid cells in a mouse system (35) we re-examined chromosome segregation in IP_8-less *asp1*^{D333A} yeast strains. Time lapse images of *asp1*^{D333A} cells expressing cen1-GFP (marks chromosome I) *sad1*$^{+}$*-mCherry* (marks the spindle pole bodies) (36, 37) revealed several mitotic cells that had an aberrant number of cen1-GFP signals (Fig 5A). *S. pombe* is a haploid organism, thus during mitosis two segregating cen1-GFP signals representing the two chromosome I sisters are observed (36). In the photomicrographs in Figure 5A, up to 6 cen1-GFP signals were observed suggesting

that these cells were polyploid. We therefore analyzed the ploidy state of wild-type, *asp1*^{D333A}, *bub3Δ*, and *asp1*^{D333A} *bub3Δ* strains via FACS analysis (Fig 5B). As shown in Figure 5C, *asp1*^{D333A} cell populations contain cells with an abnormally high DNA content (P2 population). This phenotype is increased in a *bub3Δ* background (Fig 5C). P2 cells were longer and wider (on average 15 %) compared to the entire cell population.

Intracellular IP_8 levels are increased in strains without functional Asp1 pyrophosphatase

Expression of plasmid-encoded *asp1*$^{365-920}$ negatively affected intracellular IP_8 levels while *asp1*$^{365-920/H397A}$ expression had no effect. Consequently one would expect, that a strain with an endogenous full-length *asp1* variant with a mutation at position 397 i.e. *asp1*^{H397A} (Fig 6A) generates more IP_8 than a wild-type strain. The HPLC profile of the *asp1*^{H397A} strain (endogenous *asp1*$^{+}$ ORF replaced by *asp1*^{H397A} (9)) showed a considerable increase of the IP_8 peak compared with the wild-type *asp1*$^{+}$ strain (Fig 6B-D, quantification in 6E).

Next, we investigated the consequences of loss of the entire Asp1 pyrophosphatase domain on IP_8 pools. For this we analyzed a strain which expressed an endogenous *asp1*-deletion variant consisting only of the Asp1 kinase domain Asp1$^{1-364}$ (Fig 6A). The inositol polyphosphate profile of the *asp1*$^{1-364}$ strain also showed significantly higher IP_8 levels (Fig 6F-G, quantification 6H). The similarity of the inositol polyphosphate profiles of the *asp1*^{H397A} and *asp1*$^{1-364}$ mutant strains demonstrates that the change in IP_8 levels observed for the *asp1*^{H397A} strain is solely due to the missing pyrophosphatase activity.

All conserved residues of the M1 phosphatase motif are essential for enzymatic function

We have shown previously that bacterially produced, recombinant Asp1 protein generated IP_7 *in vitro* using IP_6 as a substrate (10). The addition of $Asp1^{365-920}$ to such a kinase assay reduced the IP_7 amount in a dose-dependent manner. However, addition of $Asp1^{365-920/H397A}$ had no effect demonstrating that this Asp1 pyrophosphatase variant had no enzymatic activity (10). To determine the role of the two other conserved amino acids of the M1 motif, we exchanged the arginine residues R396 and R400 to alanine individually (Fig 7A) and tested the ability of these mutants to dephosphorylate Asp1 kinase generated IP_7 *in vitro*. It had been reported that recombinant bacterially expressed Asp1 is capable of incorporating an iron-sulfur cluster and that the presence of these iron-sulfur clusters inhibits the pyrophosphatase activity (29). Thus, we assessed the content of iron-sulfur clusters for all bacterially produced, recombinant Asp1 variants and found that our protein samples contain no iron-sulfur clusters (Fig S3A).

Recombinant GST-$Asp1^{365-920/R396A}$, GST-$Asp1^{365-920/R400A}$, GST-$Asp1^{365-920}$ and GST-$Asp1^{365-920/H397A}$ proteins were generated in bacteria and the activity of these four Asp1 variants tested in an *in vitro* pyrophosphatase assay. First, the IP_7 substrate for the assay was synthesized using the Asp1 kinase domain ($Asp1^{1-364}$), which was heat-inactivated after the reaction. Second, Asp1 pyrophosphatase variants were added to the mixture and incubated. The inositol polyphosphates present were then analyzed by PAGE (38). As shown previously (10) wild-type $Asp1^{365-920}$ massively reduced the amount of IP_7 (Fig 7B, lane 2 versus input in lane 1) while the presence of $Asp1^{364-920/H397A}$ did not (Fig 7B, lane 3). Similarly, GST-$Asp1^{365-920/R396A}$ and GST-$Asp1^{365-920/R400A}$ were unable to reduce the amount of IP_7 in our assay (Fig 7B lanes 5

242 and 4, respectively) demonstrating that all conserved residues of the M1 motif were
243 essential for *in vitro* enzymatic activity.

244 To investigate the *in vivo* function of Asp1$^{365\text{-}920/R396A}$ and Asp1$^{365\text{-}920/R400A}$, the TBZ
245 sensitivity of a wild-type strain expressing *asp1*$^{365\text{-}920/R396A}$ or *asp1*$^{365\text{-}920/R400A}$ on a
246 plasmid via the *nmt1*$^{+}$ promoter was examined. Western blot analysis showed that
247 expression levels of these Asp1$^{365\text{-}920}$ variants were similar (Fig S2). In contrast to
248 Asp1$^{365\text{-}920}$ neither Asp1$^{365\text{-}920/R396A}$ nor Asp1$^{365\text{-}920/R400A}$ increased TBZ sensitivity of
249 the strain (Fig 7C).

250 Previously, we had shown that an ***asp1Δ*** strain was hypersensitive to TBZ and that
251 this phenotype was rescued by plasmid-borne high level expression of either wild-
252 type *asp1*$^{+}$ or *asp1*^{R396A} (10). To analyze if Asp1^{R400A} could rescue the TBZ
253 hypersensitivity of the ***asp1Δ*** strain, we expressed this *asp1*$^{+}$ version in the ***asp1Δ***
254 strain. However high expression of *asp1*^{R400A} led to cell death by lysis (Fig 7D, data
255 not shown). The molecular basis for the lethality is unclear, however we and others
256 had shown previously that plasmid-borne high expression of *asp1*^{H397A} was also
257 lethal due to cell lysis (2, 10).

258 Low-level expression of *asp1*^{R400A} did not affect cell growth (Fig 7D). Thus we
259 determined if low-level expression of *asp1*^{R400A} could rescue the inability of the ***asp1Δ***
260 strain to switch to pseudohyphal invasive growth (9). This phenotype cannot be
261 rescued by plasmid-encoded wild-type *asp1*$^{+}$ under low level expression conditions
262 (Fig 7E). However low-level expression of either *asp1*^{H397A} *or asp1*^{R400A} gave rise to
263 invasively growing colonies (Fig 7E and quantification in Fig 7F). We conclude that
264 Asp1^{R400A} is able to generate more IP_8 than the wild-type Asp1 protein.

Thus all three conserved amino acids of the histidine acid phosphatase M1 motif **RH**AD**R** are essential for Asp1 pyrophosphatase activity.

Isoleucine 808 is critical for Asp1 pyrophosphatase function

Histidine acid phosphatases require the presence of an aspartate in the M2 motif HD as proton donor during the enzymatic reaction (28). No aspartate is found at this position in any Vip1 family member; in Asp1 an isoleucine residue is present at this position. To determine if an exchange to aspartate at this positon influences pyrophosphatase activity, we assayed if Asp1$^{365\text{-}920/I808D}$ (Fig 8A) could dephosphorylate IP_7 in our *in vitro* assay. This was not the case (Fig 8B).

Furthermore expression of plasmid-borne *asp1*$^{365\text{-}920/I808D}$ did not cause TBZ hypersensitivity (Fig 8C). To test if intracellular IP_8 levels were affected by the mutation at position 808 of Asp1, we constructed a strain in which the endogenous *asp1*$^{+}$ gene was replaced by *asp1*^{I808D}. Interestingly, this strain was more resistant to TBZ than a wild-type strain, similar to the *asp1*^{H397A} strain (Fig 8D) showing that the Asp1^{I808D} pyrophosphatase domain was non-functional.

Using HPLC-based analysis of inositol polyphosphates, we determined cellular IPP levels of the *asp1*^{I808D} strain. IP_8 was increased approximately twofold in the *asp1*^{I808D} strain compared to a wild-type strain (Fig 8E-G). Therefore, alteration of amino acid 808 of Asp1 to aspartate, which is the proton donor in classical histidine acid phosphatases, abolished pyrophosphatase function.

Finally we analyzed the function of the conserved histidine of the M2 motif (position H807) (Fig 8A). A publication had described this residue to be essential for pyrophosphatase function *in vitro* (29). However, expression of the *asp1*$^{365\text{-}920/H807A}$

gave rise to TBZ hypersensitivity indicating that this variant was functional (Fig S4A). We thus tested this variant in our *in vitro* pyrophosphatase assay. The addition of 8 µg of either Asp1$^{365\text{-}920}$ or Asp1$^{365\text{-}920/H807A}$ to the assay reduced IP_7, while the presence of Asp1$^{365\text{-}920/R400A}$ had no effect on IP_7 levels (Fig S4B lanes 2-4). This result shows that Asp1$^{365\text{-}920/H807A}$ still retains pyrophosphatase activity. To understand the discrepancy between our data and those of (29), we repeated the assay with 4 and 2 µg of the relevant proteins. 4 µg of protein led to a partial degradation of the IP_7 input (Fig S4B lanes 5-7) while no pyrophosphatase activity was detected when 2 µg of the proteins were used (Fig S4B lanes 9-11). Thus Asp1$^{365\text{-}920/H807A}$ retains residual pyrophosphatase activity.

Identification of *S. pombe* Met10 protein, which inhibits Asp1 pyrophosphatase activity *in vitro*

Our data show that the Asp1 protein harbors two enzymatic activities of opposing function and that MT stability and the dimorphic switch directly correlate with intracellular IP_8 levels. To find Asp1 interacting proteins that influence the function of the two domains, we conducted an extensive yeast-2-hybrid screen using pGBKT7-*asp1*$^{+}$ as bait and an *S. pombe* cDNA library constructed in the pGAD GH vector (Takara). Out of 2x 10^7 transformants (four-fold coverage of the library), 150 plasmids with putative interacting candidates were isolated and retested. One of the Asp1 interacting proteins was encoded by the uncharacterized ORF *SPCC584.01c*. which interacted specifically with the Asp1 pyrophosphatase domain (Fig 9A).

SPCC584.01c encodes a protein with a predicted size of 111.3 kDa which has 36% overall sequence identity and 52% similarity to *Saccharomyces cerevisiae* Met10, the

alpha subunit of assimilatory sulfite reductase involved in methionine and cysteine synthesis (39). Due to this similarity the ORF *SPCC584.01c* was named *met10*$^{+}$ in the *S. pombe* database PomBase and thus we refer to the protein as Met10.

To analyze if the *S. pombe* Met10 protein had a similar function to that described for *S. cerevisiae* Met10, we analyzed the growth behavior of an *S. pombe* ***met10Δ*** (deletion of *met10*$^{+}$ ORF) strain. The ***met10Δ*** strain required cysteine and methionine in the media for growth (Fig 9B) which is also the phenotype of the *S. cerevisiae* *MET10* deletion strain (40). Plasmid-borne overexpression of *met10*$^{+}$ was lethal in the wild-type strain (Fig 9C). However, overexpression of *met10*$^{+}$ was not lethal in the ***asp1Δ*** strain (Fig 9D), indicating that the lethal phenotype requires the presence of Asp1. Thus, *asp1*$^{+}$ and *met10*$^{+}$ interact genetically. We tried to co-immunoprecipitate Asp1 and Met10 proteins in a strain where the *met10*$^{+}$ ORF had been fused with *gfp* using a GFP antibody followed by western blot analysis with a polyclonal Asp1 antibody (41). However, co-immunoprecipitation using exponentially growing cells was not successful. Thus we used far western blot analysis to determine whether Met10 and Asp1$^{365\text{-}920}$ interact. Recombinantly produced and purified GST-Met10 interacted with His-Asp1$^{365\text{-}920}$, demonstrating that the proteins can bind to each other (Fig 9E).

We next analyzed the subcellular localization of the Met10-GFP protein. Photomicroscopic analysis showed that Met10-GFP was associated with tubular-like structures as has been observed for mitochondria (42). Staining of Met10-GFP cells with the mitochondria specific dye Mitotracker revealed co-localization (Fig 10A). Thus Asp1 can associate with a protein that co-localizes with mitochondria. Interestingly, in a screen for genes needed for survival under oxidative stress conditions numerous genes related to mitochondrial function were identified and the

338 *asp1*$^{+}$ ORF was one of the candidates (43). Indeed we found that mitochondria
339 distribution depended on functional Asp1 kinase. In *S. pombe* the mitochondria
340 network is comprised of interconnected tubular-like structures that are MT associated
341 (42), which guarantees proper mitochondria positioning and inheritance (44). We
342 found that in an ***asp1Δ*** strain mitochondrial distribution was abnormal. Visualization
343 of mitochondria via the mitochondria inner membrane protein Cox4-RFP (44) showed
344 that in the *asp1*$^{+}$ or *asp1*^{H397A} strain background, 83 % and 96 % of cells showed the
345 normal tubular-like mitochondrial structures (Fig 10B). However, this number was
346 reduced to 43% in ***asp1Δ*** cells. Instead these cells had aberrant mitochondrial
347 structures, the most prominent being aggregated mitochondria at the cell end(s) (Fig
348 10B). This phenotype has been described previously for mutant *mmb1* cells (44). The
349 Mmb1 protein attaches the tubular mitochondria to the MT cytoskeleton (44).
350 Intriguingly, when we expressed *asp1* variants with a functional pyrophosphatase
351 domain in an *mmb1Δ* (deletion of *mmb1*$^{+}$ ORF) strain on a plasmid, the strains were
352 unable to survive (data not shown). Thus, Asp1-generated IP_8 has a role in
353 mitochondrial function/organization.

354 To determine if Met10 affects Asp1 pyrophosphatase function, bacterially produced,
355 recombinant GST-Met10 was added to an Asp1$^{365\text{-}920}$ containing *in vitro*
356 pyrophosphatase assay. As the *S. cerevisiae* Met10 protein interacts with the
357 cytoplasmic iron-sulfur assembly (CIA) component Mms19 (alias Met18) that is
358 required for Fe-S protein maturation and is also a target of this complex, we first
359 determined if the recombinant GST-Met10 protein contained an iron-sulfur cluster
360 (45). This was not the case (Fig S3B).

361 As shown previously, the presence of GST-Asp1$^{365\text{-}920}$ in the pyrophosphatase assay
362 resulted in dephosphorylation of IP_7 (Fig 10C, lane 2). However, in the presence of

equimolar amounts of GST-Met10 and GST-Asp1$^{365-920}$ in the assay, IP_7 was not dephosphorylated (Fig 10C, lane 3). Thus, Met10 inhibits the function of the Asp1 pyrophosphatase domain. As both proteins were GST tagged and GST-GST interactions can occur, we repeated the assay using Asp1$^{365-920}$-His and GST-Met10. Again, Asp1$^{365-920}$-His dephosphorylated IP_7 but not in the presence of GST-Met10 (Fig 10C, lanes 4 and 5). Thus, *in vitro* the Met10 protein is an inhibitor of the Asp1 pyrophosphatase activity. To determine, whether the inhibitory effect of Met10 was specific for Asp1 pyrophosphatase, we tested if Met10 could inhibit another protein with pyrophosphatase activity. For this purpose recombinant GST-Ddp1 was generated and used in our *in vitro* assay. The *S. cerevisiae* Ddp1 protein has inositol pyrophosphatase activity (25). Ddp1 enzymatic activity dephosphorylated IP_7 (Fig 10C, lane 6 and 7) and this ability was not altered in the presence of equimolar amounts of GST-Met10 (Fig 10C, lane 7). Thus, *in vitro* Met10 inhibits specifically Asp1$^{365-920}$ pyrophosphatase activity. However as the inositol polyphosphate profiles of wild-type and *met10Δ* strains were similar, loss of Met10 was not sufficient to significantly down-regulate Asp1 pyrophosphatase activity *in vivo* (data not shown).

Discussion

In this work, we have established that Asp1 is a bi-functional enzyme *in vivo* responsible for the synthesis and hydrolysis of one specific inositol pyrophosphate: IP_8. Functional dissection of the Asp1 pyrophosphatase by mutational analysis combined with our previous analysis of Asp1 function demonstrated that morphogenesis and chromosome transmission are regulated by IP_8 in a dose dependent manner (9, 10, 12). In fact a direct correlation exists for the optimization of a cellular process and IP_8 levels: for example, higher-than-wild-type IP_8 levels resulted in higher-than-wild-type chromosome transmission fidelity. On the other hand, strains with less-than-wildtype or no IP_8 showed decreased chromosome transmission fidelity (12). The output of the Asp1 kinase is counter steered by the Asp1 pyrophosphatase, thus up- or down-regulation of pyrophosphatase activity controls intracellular IP_8 levels.

Identification of conserved amino acids essential for pyrophosphatase function

We were the first to show in an *in vitro* assay that a member of the PPIP5Ks/Vip1 family proteins has pyrophosphatase activity: IP_7 produced by the Asp1 kinase was reduced by $Asp1^{365\text{-}920}$ demonstrating that the C-terminal Asp1 domain was enzymatically active (10). Pyrophosphatase activity depended on the two conserved signature motifs of histidine acid phosphatases M1 and M2. The conserved amino acids of M1 were essential for enzymatic function of the Asp1 pyrophosphatase *in vitro* and *in vivo.* Similarly, our *in vivo* read-out assays for strains expressing *asp1* variants with the mutation R396A or R400A imply that these are also

403 pyrophosphatase negative (10). In metazoans, a mutation in either PPIP5K protein
404 complementary to the Asp1^{R396} mutation had a similar effect (46).

405 Of particular interest was the second amino acid of the M2 motif HD as this amino
406 acid is not conserved in PPIP5Ks/Vip1 family members (1). For Asp1 the M2 motif is
407 HI. The catalytic mechanism of histidine acid phosphatases requires a proton donor,
408 which is typically a glutamate or aspartate residue proximal to the active site (28).
409 Replacement of the glutamate/aspartate residue resulted in a dramatic decrease of
410 enzymatic activity (47, 48). Thus it was of great interest to determine the enzymatic
411 activity of a mutant Asp1 variant where the wild-type isoleucine had been replaced by
412 aspartate resulting in the "perfect" M2 signature motifs of histidine acid
413 phosphatases. Asp1^{I808D} variants had no *in vitro* and *in vivo* pyrophosphatase
414 activity. Furthermore, replacement of isoleucine 808 by valine, which is found at this
415 position in metazoan PPIP5Ks/Vip1 family members also led to inactivation of
416 pyrophosphatase function (data not shown) (1, 3).

417 Finally, the histidine in the M2 motif is conserved in histidine acid phosphatases and
418 all PPIP5Ks/Vip1 family members (1). A previous publication showed that mutation of
419 this residue generating Asp1$^{397\text{-}920/H807A}$ led to a loss of about 95% activity *in vitro*
420 (29). However, we found that Asp1$^{365\text{-}920/H807A}$ retained residual pyrophosphatase
421 activity. The different results obtained might be due to a different experimental set-up.
422 Interestingly, it has been shown for the rat fructose 2,6 bisphosphatase that the
423 replacement of the equivalent histidine did not significantly change the enzymatic
424 activity (49).

425

426 Cellular levels of IP_8 are regulated by Asp1 pyrophosphatase activity

Ectopic expression of *asp1*$^{365-920}$ massively reduced cellular IP_8 amounts while endogenous pyrophosphatase-dead variants increased cellular IP_8 levels. Thus, intracellular IP_8 levels can be up- or down-regulated by the enzymatic activity of the Asp1 pyrophosphatase domain. These high energy molecules are generated solely by the Asp1 kinase domain as *asp1Δ* and *asp1*^{D333A} strains had no detectable IP_8 (2, 9, 10). Similarly, *S. cerevisiae* and *C. neoformans* strains with a deletion of the gene, which encodes the PPIP5Ks/Vip1 protein, have no or massively reduced IP_8 levels but elevated IP_7 levels implying that in these organisms PPIP5Ks/Vip1 proteins generate IP_8 (6, 11, 20). The *in vivo* function of the pyrophosphatase domain of PPIP5Ks/Vip1 proteins in other organisms remains to be studied.

The Asp1 interacting protein Met10 inhibits the pyrophosphatase activity *in vitro*

We identified the mitochondria-associated Met10 protein that specifically interacted with the Asp1 pyrophosphatase domain and inhibited its function *in vitro*. Met10 belongs to a conserved protein family involved in the methionine biosynthesis pathway. Interestingly, the *S. cerevisiae* Met10 member interacts physically with the highly conserved Mms19 (alias Met18) protein (45). Mms19, which was identified previously to be also required for methionine biosynthesis, has since been shown to be a member of the Fe-S protein assembly (CIA) machinery (45, 50, 51). Incorporation of iron-sulfur clusters into proteins is mediated by a two-step mechanism occurring in the mitochondria and the cytosol (reviewed in (52)). Mms19 serves as part of a CIA targeting complex responsible for iron-sulfur cluster insertion into proteins involved in specific cellular processes including methionine biosynthesis (45). Mms19 is needed for the sulfite reductase activity of the *S. cerevisiae* Met5-

Met10 complex where Met10 represents a Fe-S containing protein (45). As the Asp1 pyrophosphatase activity is inhibited by the incorporation of an iron-sulfur cluster *in vitro* (29), it is possible that such an iron-sulfur cluster transfer could occur via *S. pombe* Met10 *in vivo*. However, the consequences of such a transfer *in vivo* remain unclear. Inositol polyphosphate profiles of wild-type and *met10Δ* strains were comparable and expression of an *asp1* variant where one of the cysteine residues required for binding the iron-sulfur cluster was mutated (29), had no phenotypic consequences for yeast cell growth under varying conditions (data not shown).

IP_8 and its impact on the microtubule cytoskeleton

The human MMS19 protein is part of the 5 component MMXD complex required for chromosome transmission fidelity. MMS19 localizes to the mitotic spindle and a knockdown of MMS19 gave rise to highly abnormal spindles (53). Thus, MMS19 is required for spindle formation/function. We have previously shown that *S. pombe* Asp1 kinase function controls bipolar spindle formation by modulating in- and outward pulling forces at the spindle (12). Our results raise the intriguing possibility that IP_8 modulated MT regulation might involve the Met10-Mms19 pathway. Although the impact of the Mms19 protein on the MT cytoskeleton has not been tested in *S. pombe*, it has been found that *S. pombe* cells with a deletion of the *mms19*$^+$ encoding gene have an abnormal cell shape showing branched and curved cells (54). Such cell shapes are indicative of a defective interphase MT cytoskeleton (reviewed in (55)). Furthermore a *S. cerevisiae met10Δ bim1Δ* double mutant strain is non-viable (56). *Bim1* is a part of the EB1 family, which represents a central element of polymerizing MT plus-ends (57). Thus, it is feasible that the Met10 and Mms19 proteins play a role in MT modulation.

Central elements in bipolar spindle assembly/function and segregation of spindle poles are kinesin-5 family members (58). The human kinesin-5 Eg5 protein has been in the focus of research due to its important role in tumorigenesis. This motor protein is up-regulated in many types of cancer such as pancreatic cancer, is associated with poor prognosis and can trigger genome instability in the mouse system (34, 35, 59). It is thus of great interest that intracellular IP_8 levels control spindle association of the *S. pombe* kinesin-5 Cut7. This finding raises the exciting possibility that IP_8 levels could be used as a tool to control Eg5 up-regulation.

Materials and Methods

Strains, plasmids and media

All strains used are listed in Table 1. Generation of *asp1* mutant strains was performed as described (9). Gene deletions and ORF fusions to *gfp* were done by PCR-based gene targeting (60) using the kanamycin resistance (kan^R) cassette. $asp1^+$, $asp1^{1\text{-}364}$, $asp^{365\text{-}920}$ plasmids are derivatives of pJR2-3XL (9, 12, 61). For the $asp1^{365\text{-}920/H397A}$, $asp1^{365\text{-}920/H807A}$, $asp1^{365\text{-}920/R396A}$, $asp1^{365\text{-}920/R400A}$, $asp1^{365\text{-}920/I808D}$ containing plasmids, PCR fragments were generated by directed mutagenesis using the QuikChangeII Site-Directed Mutagenesis Kit (Agilent Technologies) and cloned into pJR2-3XL (61) via homologous recombination in *S. cerevisiae* (62).

S .pombe strains were grown in rich media (YE5S) or minimal media (MM) with supplements (63). To control the $nmt1^+$ promoter, cells were grown in MM with or without 5 µg/ml thiamine. Experiments were carried out at 25°C, except the invasive growth experiments and the labeling with [^{3}H]inositol which were performed at 30°C. Microscopy was performed at temperatures stated in the respective figure legends.

Western blot analysis

Transformants with plasmid-borne expression of *asp1* variants were grown under plasmid selective conditions without thiamine for 24 h at 25°C before protein extraction. Protein extraction was carried out as described (9) using an anti-GFP antibody when *asp1* variants were fused to *gfp* (monoclonal mouse; Roche) or using an anti-Asp1 antibody (41) and an anti-γ-tubulin antibody (monoclonal mouse; Sigma).

In vitro enzymatic activity of Asp1 variants

Recombinant proteins *Asp1$^{1-364}$ and Asp1$^{365-920}$* were previously described (10). 1751 bp PCR fragments containing *asp1$^{365-920/R396A}$, asp1$^{365-920/H397A}$, asp1$^{365-920/R400A}$, asp1$^{365-920/H807A}$*, *asp1$^{365-920/I808D}$, 3101 bp* fragment containing the entire *met10^{+}* ORF or 649 bp fragment containing the entire ScDDP1 ORF were cloned into *E. coli* expression vector pKM36 to generate GST-tagged proteins or into *E. coli* expression vector pFT25 to generate His-tagged proteins. Proteins were expressed and purified from *E. coli* Rosetta (DE3) strain according to protocol (Sigma Aldrich). Enzymatic reactions were performed as described (10, 38). For the kinase reaction, 4 µg of purified Asp1$^{1-364}$ protein was incubated for 16 h at 37°C with 300 µM IP_6 (Sigma-Aldrich) followed by Asp1$^{1-364}$ inactivation (65°C for 20 min). Inactivation was verified by performing a kinase assay with the treated Asp1$^{1-364}$ protein. 30 µl of the generated IP_7 were incubated with 8 µg of Asp1$^{365-920}$ variants for 16 h at 37°C, followed by PAGE analysis. In Fig 10C, 8 µg of GST-Met10, 2 µg of GST-Ddp1 and 4 µg of Asp1$^{365-920}$ were used in the assay.

[^{3}H]inositol labeling and HPLC analysis.

[^{3}H]inositol labeling of *S. pombe* cultures was performed as described (31). Cells were grown overnight at 30°C in MM with 55 µM inositol followed by dilution to OD_{600} of 0.05 in 5 ml MM with 10 µM inositol supplemented with 6 µCi/ml of [^{3}H]inositol and incubated until OD_{600} reached 0.8-1.6 (30 to 48 h). Extraction of inositol polyphosphates was performed as described (31) and resolved by anion exchange chromatography HPLC (using the partisphere SAX 4.6 × 125 mm column; Whatman).

Collected fractions were analyzed by scintillation counting. Soluble inositol polyphosphate levels were normalized against total lipid inositol content. Statistics for the ratios of IP_8/ IP_6, IP_8/IP_7 and IP_7/ IP_6 were performed using Graphpad Prism 5.

Electronic absorption spectroscopy

Electronic absorption spectroscopy was used to determine the iron-sulfur cluster content of $Asp1^{365-920}$. Electronic absorption spectra were recorded using a double-beam JASCO V-650 spectrophotometer at room temperature. Spectra were obtained using a 1 cm path length cuvette for samples with a protein concentration of ~1 µg /ml.

Flow cytometry

Yeast flow cytometry was carried out as described using Sytox green (64) and a FACS Aria (BD Biosciences). 10000 cells were counted/ sample and all strains were counted at least twice and were grown at different temperatures before fixation (20-36 °C). The data shown in Fig 5B-C was obtained from cells incubated at 30 °C but is representative for all other temperatures. DNA content of cells was defined using the temperature sensitive *cdc11-123* strain as a standard (65).

Invasive growth assay

Transformants were grown overnight in plasmid selective media with or without thiamine. Cells were diluted to an end concentration of $2x\ 10^6$ cells/ml and 5 µl of cells were patched on plasmid selective agar plates at equal distance from each other. Incubation was done at 30°C for 21 days (66). To analyze invasive growth,

surface grown cells were removed by washing, plates were dried and then photographed using a binocular microscope and digital Sony DSLR camera. Quantification of invasive growth was done by determining the number of invasive colonies per mutant in 3 different transformants in at least 3 different experiments.

Yeast 2-hybrid screen

Yeast-2-hybrid screen was performed using the AH109 strain transformed with pGBKT7-*asp1*$^{+}$ as bait and mated with Y187 transformed with an *S. pombe* cDNA library constructed in the pGAD GH vector (MATCHMAKER cDNA Library (XL4000AA Takara). Mating was plated on SD-Leu-Trp-His and incubated for 8 days. Plasmids from positive candidates were co-transformed with pGBKT7-*asp1*$^{+}$ into strain AH109 and further analyzed.

Microscopy

Live-cell imaging was performed using a Zeiss spinning-disk confocal microscope equipped with a Rolera EM-C (QImaging) camera. Transformants expressing *cut7*$^{+}$*-GFP* were pre-grown for 20 h at 30°C in plasmid selective media. Videos were taken at 30°C. For *asp1*$^{+}$ *cut7*$^{+}$*-GFP* and *asp1*^{D333A} *cut7*$^{+}$*-GFP* strains growth and imaging was done at 33°C. A maximum intensity projection (MIP) picture (25 z-slices (transformants) or 35 z-slices (strains) in 0.5 µm intervals) of the time point with the strongest fluorescence signal on a short spindle was generated and used for analysis. Analysis was performed using Zen2012 and Axiovision software. Image processing was done with Canvas 14 and Adobe Photoshop CS2. Intensity of GFP fluorescence signals was measured via ImageJ 1.44 (NIH). The *asp1*^{D333A} *bub3Δ*

strain was pre-grown for 24 h at 30°C. Shown in Fig 5A are MIP images of a single cell. For live-cell imaging of *met10*$^{+}$*-GFP* expressing cells stained with Mitotracker or *cox4*$^{+}$*-RFP* cells expressing different *asp1* variants, cells were recorded at 25 °C with a z-stack of 25 z-slices with a distance of 0.5 µm and a MIP image generated. Statistics for fluorescence signal intensity ratios and spindle break frequencies were performed using Graphpad Prism 5.

Far-Western blot analysis

GST-Met10 and Asp1$^{365\text{-}920}$-His were purified from the *E. coli* Rosetta (DE3) strain. 1 µg of GST-Met10 or Asp1$^{365\text{-}920}$-His (prey proteins) were separated by 10% SDS-PAGE and then transferred to a PVDF membrane. After denaturation with 6 M guanidine-HCl, the prey protein was gradually renatured on the membrane by incubation with decreasing concentrations of guanidine-HCl in a buffer containing Glycerin 10% , 0.1 M NaCl, 20 mM Tris pH 7.5, 1 mM EDTA, 0.1 % Tween-20, 2% milk and 1 mM DTT. After an overnight incubation at 4°C with the buffer containing no guanidine-HCl, 10 µg/ml of Asp1$^{365\text{-}920}$-His, GST-Met10 or GST (bait proteins) were incubated 5 h at RT with the regenerated membrane. After 3 washes with PBS, protein interactions were detected using His (Roche) or GST (Thermo Fisher) antibodies.

Acknowledgements

We thank Boris Topolski for his help with Figure 4B and Katja Mölleken and Tim Fechtner for plasmids (all Heinrich-Heine University, Düsseldorf, Germany), Phong Tran (University of Pennsylvania, USA) for strains, Klaus Meyer (Heinrich-Heine University, Düsseldorf, Germany) for help with the FACS analysis and Anna Feoktistova and Kathleen Gould (Vanderbilt University, Nashville, USA) for the very generous gift of Asp1 antibody. We thank the Center for Advanced Imaging (CAi) at the Heinrich-Heine-University. This work was supported by the Deutsche Forschungsgemeinschaft (http://www.dfg.de/): project FOR1334 and the Manchot Graduate school MOI II (Juergen Manchot Stiftung) to UF; Fonds der Chemischen Industrie to IS and Medical Research Council (MRC) core support to the MRC/UCL Laboratory for Molecular Cell Biology University Unit (MC_UU_1201814) to AS.

Funding Information

The funders had no role in study design, data collection and interpretation, or the decision to submit the work for publication.

References

1. Fridy PC, Otto JC, Dollins DE, York JD. 2007. Cloning and characterization of two human VIP1-like inositol hexakisphosphate and diphosphoinositol pentakisphosphate kinases. J Biol Chem 282:30754-62.
2. Mulugu S, Bai W, Fridy PC, Bastidas RJ, Otto JC, Dollins DE, Haystead TA, Ribeiro AA, York JD. 2007. A conserved family of enzymes that phosphorylate inositol hexakisphosphate. Science 316:106-9.
3. Choi JH, Williams J, Cho J, Falck JR, Shears SB. 2007. Purification, sequencing, and molecular identification of a mammalian PP-InsP5 kinase that

is activated when cells are exposed to hyperosmotic stress. J Biol Chem 282:30763-75.

4. Saiardi A, Resnick AC, Snowman AM, Wendland B, Snyder SH. 2005. Inositol pyrophosphates regulate cell death and telomere length through phosphoinositide 3-kinase-related protein kinases. Proc Natl Acad Sci U S A 102:1911-4.

5. York SJ, Armbruster BN, Greenwell P, Petes TD, York JD. 2005. Inositol diphosphate signaling regulates telomere length. J Biol Chem 280:4264-9.

6. Laha D, Johnen P, Azevedo C, Dynowski M, Weiss M, Capolicchio S, Mao H, Iven T, Steenbergen M, Freyer M, Gaugler P, de Campos MK, Zheng N, Feussner I, Jessen HJ, Van Wees SC, Saiardi A, Schaaf G. 2015. VIH2 Regulates the Synthesis of Inositol Pyrophosphate InsP8 and Jasmonate-Dependent Defenses in Arabidopsis. Plant Cell 27:1082-97.

7. Pulloor NK, Nair S, Kostic AD, Bist P, Weaver JD, Riley AM, Tyagi R, Uchil PD, York JD, Snyder SH, Garcia-Sastre A, Potter BV, Lin R, Shears SB, Xavier RJ, Krishnan MN. 2014. Human genome-wide RNAi screen identifies an essential role for inositol pyrophosphates in Type-I interferon response. PLoS Pathog 10:e1003981.

8. Chakraborty A, Koldobskiy MA, Bello NT, Maxwell M, Potter JJ, Juluri KR, Maag D, Kim S, Huang AS, Dailey MJ, Saleh M, Snowman AM, Moran TH, Mezey E, Snyder SH. 2010. Inositol pyrophosphates inhibit Akt signaling, thereby regulating insulin sensitivity and weight gain. Cell 143:897-910.

9. Pöhlmann J, Fleig U. 2010. Asp1, a conserved 1/3 inositol polyphosphate kinase, regulates the dimorphic switch in Schizosaccharomyces pombe. Mol Cell Biol 30:4535-47.

10. Pöhlmann J, Risse C, Seidel C, Pohlmann T, Jakopec V, Walla E, Ramrath P, Takeshita N, Baumann S, Feldbrugge M, Fischer R, Fleig U. 2014. The Vip1 inositol polyphosphate kinase family regulates polarized growth and modulates the microtubule cytoskeleton in fungi. PLoS Genet 10:e1004586.

11. Lev S, Li C, Desmarini D, Saiardi A, Fewings NL, Schibeci SD, Sharma R, Sorrell TC, Djordjevic JT. 2015. Fungal Inositol Pyrophosphate IP7 Is Crucial for Metabolic Adaptation to the Host Environment and Pathogenicity. MBio 6:e00531-15.

12. Topolski B, Jakopec V, Kunzel NA, Fleig U. 2016. Inositol Pyrophosphate Kinase Asp1 Modulates Chromosome Segregation Fidelity and Spindle Function in Schizosaccharomyces pombe. Mol Cell Biol 36:3128-3140.
13. Lee YS, Mulugu S, York JD, O'Shea EK. 2007. Regulation of a cyclin-CDK-CDK inhibitor complex by inositol pyrophosphates. Science 316:109-12.
14. Saiardi A, Bhandari R, Resnick AC, Snowman AM, Snyder SH. 2004. Phosphorylation of proteins by inositol pyrophosphates. Science 306:2101-5.
15. Wu M, Chong LS, Perlman DH, Resnick AC, Fiedler D. 2016. Inositol polyphosphates intersect with signaling and metabolic networks via two distinct mechanisms. Proc Natl Acad Sci U S A 113:E6757-E6765.
16. Draskovic P, Saiardi A, Bhandari R, Burton A, Ilc G, Kovacevic M, Snyder SH, Podobnik M. 2008. Inositol hexakisphosphate kinase products contain diphosphate and triphosphate groups. Chem Biol 15:274-86.
17. Saiardi A, Erdjument-Bromage H, Snowman AM, Tempst P, Snyder SH. 1999. Synthesis of diphosphoinositol pentakisphosphate by a newly identified family of higher inositol polyphosphate kinases. Curr Biol 9:1323-6.
18. Wang H, Falck JR, Hall TM, Shears SB. 2011. Structural basis for an inositol pyrophosphate kinase surmounting phosphate crowding. Nat Chem Biol 8:111-6.
19. Lin H, Fridy PC, Ribeiro AA, Choi JH, Barma DK, Vogel G, Falck JR, Shears SB, York JD, Mayr GW. 2009. Structural analysis and detection of biological inositol pyrophosphates reveal that the family of VIP/diphosphoinositol pentakisphosphate kinases are 1/3-kinases. J Biol Chem 284:1863-72.
20. Onnebo SM, Saiardi A. 2009. Inositol pyrophosphates modulate hydrogen peroxide signalling. Biochem J 423:109-18.
21. Gu C, Wilson MS, Jessen HJ, Saiardi A, Shears SB. 2016. Inositol Pyrophosphate Profiling of Two HCT116 Cell Lines Uncovers Variation in InsP8 Levels. PLoS One 11:e0165286.
22. Luo HR, Huang YE, Chen JC, Saiardi A, Iijima M, Ye K, Huang Y, Nagata E, Devreotes P, Snyder SH. 2003. Inositol pyrophosphates mediate chemotaxis in Dictyostelium via pleckstrin homology domain-PtdIns(3,4,5)P3 interactions. Cell 114:559-72.

694 23. Pesesse X, Choi K, Zhang T, Shears SB. 2004. Signaling by higher inositol
695 polyphosphates. Synthesis of bisdiphosphoinositol tetrakisphosphate ("InsP8")
696 is selectively activated by hyperosmotic stress. J Biol Chem 279:43378-81.
697 24. Safrany ST, Caffrey JJ, Yang X, Bembenek ME, Moyer MB, Burkhart WA,
698 Shears SB. 1998. A novel context for the 'MutT' module, a guardian of cell
699 integrity, in a diphosphoinositol polyphosphate phosphohydrolase. Embo J
700 17:6599-607.
701 25. Lonetti A, Szijgyarto Z, Bosch D, Loss O, Azevedo C, Saiardi A. 2011.
702 Identification of an evolutionarily conserved family of inorganic polyphosphate
703 endopolyphosphatases. J Biol Chem 286:31966-74.
704 26. Fisher DI, Safrany ST, Strike P, McLennan AG, Cartwright JL. 2002. Nudix
705 hydrolases that degrade dinucleoside and diphosphoinositol polyphosphates
706 also have 5-phosphoribosyl 1-pyrophosphate (PRPP) pyrophosphatase
707 activity that generates the glycolytic activator ribose 1,5-bisphosphate. J Biol
708 Chem 277:47313-7.
709 27. Steidle EA, Chong LS, Wu M, Crooke E, Fiedler D, Resnick AC, Rolfes RJ.
710 2016. A Novel Inositol Pyrophosphate Phosphatase in Saccharomyces
711 cerevisiae: Siw14 PROTEIN SELECTIVELY CLEAVES THE beta-
712 PHOSPHATE FROM 5-DIPHOSPHOINOSITOL PENTAKISPHOSPHATE
713 (5PP-IP5). J Biol Chem 291:6772-83.
714 28. Rigden DJ. 2008. The histidine phosphatase superfamily: structure and
715 function. Biochem J 409:333-48.
716 29. Wang H, Nair VS, Holland AA, Capolicchio S, Jessen HJ, Johnson MK,
717 Shears SB. 2015. Asp1 from Schizosaccharomyces pombe binds a [2Fe-
718 2S](2+) cluster which inhibits inositol pyrophosphate 1-phosphatase activity.
719 Biochemistry 54:6462-74.
720 30. Fernandez S, Homann MJ, Henry SA, Carman GM. 1986. Metabolism of the
721 phospholipid precursor inositol and its relationship to growth and viability in the
722 natural auxotroph Schizosaccharomyces pombe. J Bacteriol 166:779-86.
723 31. Azevedo C, Saiardi A. 2006. Extraction and analysis of soluble inositol
724 polyphosphates from yeast. Nat Protoc 1:2416-22.
725 32. Hagan I, Yanagida M. 1990. Novel potential mitotic motor protein encoded by
726 the fission yeast cut7+ gene. Nature 347:563-6.

33. Toya M, Sato M, Haselmann U, Asakawa K, Brunner D, Antony C, Toda T. 2007. Gamma-tubulin complex-mediated anchoring of spindle microtubules to spindle-pole bodies requires Msd1 in fission yeast. Nat Cell Biol 9:646-53.
34. Jin Q, Huang F, Wang X, Zhu H, Xian Y, Li J, Zhang S, Ni Q. 2017. High Eg5 expression predicts poor prognosis in breast cancer. Oncotarget 8:62208-62216.
35. Liu M, Wang X, Yang Y, Li D, Ren H, Zhu Q, Chen Q, Han S, Hao J, Zhou J. 2010. Ectopic expression of the microtubule-dependent motor protein Eg5 promotes pancreatic tumourigenesis. J Pathol 221:221-8.
36. Nabeshima K, Nakagawa T, Straight AF, Murray A, Chikashige Y, Yamashita YM, Hiraoka Y, Yanagida M. 1998. Dynamics of centromeres during metaphase-anaphase transition in fission yeast: Dis1 is implicated in force balance in metaphase bipolar spindle. Mol Biol Cell 9:3211-25.
37. Hagan I, Yanagida M. 1995. The product of the spindle formation gene sad1+ associates with the fission yeast spindle pole body and is essential for viability. J Cell Biol 129:1033-47.
38. Loss O, Azevedo C, Szijgyarto Z, Bosch D, Saiardi A. 2011. Preparation of quality inositol pyrophosphates. J Vis Exp doi:3027 [pii]
10.3791/3027:e3027.
39. Hansen J, Cherest H, Kielland-Brandt MC. 1994. Two divergent MET10 genes, one from Saccharomyces cerevisiae and one from Saccharomyces carlsbergensis, encode the alpha subunit of sulfite reductase and specify potential binding sites for FAD and NADPH. J Bacteriol 176:6050-8.
40. Thomas D, Surdin-Kerjan Y. 1997. Metabolism of sulfur amino acids in Saccharomyces cerevisiae. Microbiol Mol Biol Rev 61:503-32.
41. Feoktistova A, McCollum D, Ohi R, Gould KL. 1999. Identification and characterization of Schizosaccharomyces pombe asp1(+), a gene that interacts with mutations in the Arp2/3 complex and actin. Genetics 152:895-908.
42. Yaffe MP, Harata D, Verde F, Eddison M, Toda T, Nurse P. 1996. Microtubules mediate mitochondrial distribution in fission yeast. Proc Natl Acad Sci U S A 93:11664-8.
43. Zuin A, Gabrielli N, Calvo IA, Garcia-Santamarina S, Hoe KL, Kim DU, Park HO, Hayles J, Ayte J, Hidalgo E. 2008. Mitochondrial dysfunction increases

761 oxidative stress and decreases chronological life span in fission yeast. PLoS
762 One 3:e2842.
763 44. Fu C, Jain D, Costa J, Velve-Casquillas G, Tran PT. 2011. mmb1p binds
764 mitochondria to dynamic microtubules. Curr Biol 21:1431-9.
765 45. Stehling O, Vashisht AA, Mascarenhas J, Jonsson ZO, Sharma T, Netz DJ,
766 Pierik AJ, Wohlschlegel JA, Lill R. 2012. MMS19 assembles iron-sulfur
767 proteins required for DNA metabolism and genomic integrity. Science
768 337:195-9.
769 46. Gu C, Nguyen HN, Hofer A, Jessen HJ, Dai X, Wang H, Shears SB. 2017. The
770 Significance of the Bifunctional Kinase/Phosphatase Activities of
771 Diphosphoinositol Pentakisphosphate Kinases (PPIP5Ks) for Coupling Inositol
772 Pyrophosphate Cell Signaling to Cellular Phosphate Homeostasis. J Biol
773 Chem 292:4544-4555.
774 47. Ostanin K, Van Etten RL. 1993. Asp304 of Escherichia coli acid phosphatase
775 is involved in leaving group protonation. J Biol Chem 268:20778-84.
776 48. Lin K, Li L, Correia JJ, Pilkis SJ. 1992. Glu327 is part of a catalytic triad in rat
777 liver fructose-2,6-bisphosphatase. J Biol Chem 267:6556-62.
778 49. Mizuguchi H, Cook PF, Tai CH, Hasemann CA, Uyeda K. 1999. Reaction
779 mechanism of fructose-2,6-bisphosphatase. A mutation of nucleophilic
780 catalyst, histidine 256, induces an alteration in the reaction pathway. J Biol
781 Chem 274:2166-75.
782 50. Masselot M, De Robichon-Szulmajster H. 1975. Methionine biosynthesis in
783 Saccharomyces cerevisiae. I. Genetical analysis of auxotrophic mutants. Mol
784 Gen Genet 139:121-32.
785 51. Gari K, Leon Ortiz AM, Borel V, Flynn H, Skehel JM, Boulton SJ. 2012.
786 MMS19 links cytoplasmic iron-sulfur cluster assembly to DNA metabolism.
787 Science 337:243-5.
788 52. Netz DJ, Mascarenhas J, Stehling O, Pierik AJ, Lill R. 2014. Maturation of
789 cytosolic and nuclear iron-sulfur proteins. Trends Cell Biol 24:303-12.
790 53. Ito S, Tan LJ, Andoh D, Narita T, Seki M, Hirano Y, Narita K, Kuraoka I,
791 Hiraoka Y, Tanaka K. 2010. MMXD, a TFIIH-independent XPD-MMS19 protein
792 complex involved in chromosome segregation. Mol Cell 39:632-40.

793 54. Hayles J, Wood V, Jeffery L, Hoe KL, Kim DU, Park HO, Salas-Pino S,
794 Heichinger C, Nurse P. 2013. A genome-wide resource of cell cycle and cell
795 shape genes of fission yeast. Open Biol 3:130053.
796 55. Huisman SM, Brunner D. 2011. Cell polarity in fission yeast: a matter of
797 confining, positioning, and switching growth zones. Semin Cell Dev Biol
798 22:799-805.
799 56. Pan X, Yuan DS, Xiang D, Wang X, Sookhai-Mahadeo S, Bader JS, Hieter P,
800 Spencer F, Boeke JD. 2004. A robust toolkit for functional profiling of the yeast
801 genome. Mol Cell 16:487-96.
802 57. Beinhauer JD, Hagan IM, Hegemann JH, Fleig U. 1997. Mal3, the fission
803 yeast homologue of the human APC-interacting protein EB-1 is required for
804 microtubule integrity and the maintenance of cell form. J Cell Biol 139:717-28.
805 58. Wojcik EJ, Buckley RS, Richard J, Liu L, Huckaba TM, Kim S. 2013. Kinesin-
806 5: cross-bridging mechanism to targeted clinical therapy. Gene 531:133-49.
807 59. Castillo A, Morse HC, 3rd, Godfrey VL, Naeem R, Justice MJ. 2007.
808 Overexpression of Eg5 causes genomic instability and tumor formation in
809 mice. Cancer Res 67:10138-47.
810 60. Bahler J, Wu JQ, Longtine MS, Shah NG, McKenzie A, 3rd, Steever AB, Wach
811 A, Philippsen P, Pringle JR. 1998. Heterologous modules for efficient and
812 versatile PCR-based gene targeting in Schizosaccharomyces pombe [In
813 Process Citation]. Yeast 14:943-51.
814 61. Moreno MB, Duran A, Ribas JC. 2000. A family of multifunctional thiamine-
815 repressible expression vectors for fission yeast. Yeast 16:861-72.
816 62. Jakopec V, Walla E, Fleig U. 2011. Versatile use of Schizosaccharomyces
817 pombe plasmids in Saccharomyces cerevisiae. FEMS Yeast Res 11:653-5.
818 63. Moreno S, Klar A, Nurse P. 1991. Molecular genetic analysis of fission yeast
819 Schizosaccharomyces pombe. Methods Enzymol 194:795-823.
820 64. Sabatinos SA, Forsburg SL. 2009. Measuring DNA content by flow cytometry
821 in fission yeast. Methods Mol Biol 521:449-61.
822 65. Creanor J, Mitchison JM. 1984. Protein synthesis and its relation to the DNA-
823 division cycle in the fission yeast Schizosaccharomyces pombe. J Cell Sci
824 69:199-210.

66. Prevorovsky M, Stanurova J, Puta F, Folk P. 2009. High environmental iron concentrations stimulate adhesion and invasive growth of Schizosaccharomyces pombe. FEMS Microbiol Lett 293:130-4.

Figure Legends

Fig 1. Asp1 kinase generates IP_8.

A to **C:** HPLC elution profiles of inositol polyphosphates of wild-type (WT), *asp1*^{D333A} and *asp1Δ* strains. *S. pombe* cells were radiolabeled with [^{3}H]inositol and cell lysates separated using anion-exchange HPLC. CPM: counts per minute. **D:** Left: diagrammatic representation of IP_8 levels relative to IP_6. Right: diagrammatic representation of IP_7 levels relative to IP_6. (WT: n= 3; *asp1*^{D333A} n= 2; *asp1Δ* n= 3. ***: $P \leq 0.001$; *: $P \leq 0.05$, t-test). The fold-change of IP_8/ IP_6 is as follows: (WT set at 1.00); 0.12 (*asp1*^{D333A}*)* and 0.11 *(asp1Δ).* Fold-change of IP_7/ IP_6: 6.26 (*asp1*^{D333A}*)* and 4.56 *(asp1Δ).*

Fig 2. *In vivo* analysis of Asp1$^{365\text{-}920}$ and Asp1$^{365\text{-}920/H397A}$ function.

A: Diagrammatic representation of the dual-domain structure of Asp1 with kinase (K, black box) and pyrophosphatase (P, light grey box) regions. Enlargement of pyrophosphatase domain with the signature motifs M1 and M2 of histidine acid phosphatases (dark grey boxes) (1). In Asp1, the aspartate residue of M2 is replaced by isoleucine (H**I** instead of H**D**). **B:** Serial dilution patch tests (10^4 to 10^1 cells) of a wild-type strain transformed with vector (control) or plasmids expressing *asp1*$^{365–920}$ or *asp1*$^{365–920/H397A}$ from the thiamine-repressible promoter *nmt1*$^+$. Transformants were grown under plasmid selective conditions in absence or presence of 7 µg/ ml

TBZ at 25°C for 7 days. **C:** Invasive growth assay. Left: A total of 10^5 wild-type cells transformed with either vector control or plasmids with *asp1*$^{365–920}$ or *asp1*$^{365–920/H397A}$ were spotted on plasmid selective medium without thiamine and incubated for 21 days at 30°C (top panels, surface growth). Plates were washed and all surface growth rubbed off. Invasively growing colonies remained (bottom panels) and were counted. Quantification shown on the right: 3 transformants were analyzed per plasmid in triplicate, ns= not significant, ***: P < 0.0005, t test. The number of agar-invading colonies of the *asp1*$^{365-920/H397A}$ transformants and the control transformants were 16.5± 4.0 and 17.5± 3.6, respectively.

Fig 3. Asp1$^{365-920}$ has pyrophosphatase activity *in vivo.*

A to **C:** HPLC elution profiles of inositol polyphosphates of the wild-type strain transformed with (**A**) vector control or *asp1*$^{365–920}$ or *asp1*$^{365–920/H397A}$ expressing plasmids (**B** and **C**, respectively). Cells were radiolabeled with [^{3}H] inositol and cell lysates separated using anion-exchange HPLC. **D:** Diagrammatic representation of IP_8 levels relative to IP_6 (left) and IP_7 levels relative to IP_6 (right) normalized to the vector control using data from A, B and C**.** (control: n= 4; pasp1$^{365-920}$ n= 4; pasp1$^{365-920/H397A}$ n= 4. **: P ≤ 0.01; *: P ≤ 0.05; ns: not significant, t-test). The fold-change of IP_8/ IP_6 is as follows: (control set at 1.00); 0.4 (pasp1$^{365-920}$) and 5.3 (pasp1$^{365-920/H397A}$). Fold-change of IP_7/ IP_6: 9.3 (pasp1$^{365-920}$) and 1.8 (pasp1$^{365-920/H397A}$). **E:** MT stability and the dimorphic switch require intracellular IP_8, which are down-regulated by Asp1 pyrophosphatase activity.

Fig 4. IP_8 controls Cut7-GFP spindle association.

A: Photomicrographs of *cut7*$^{+}$*-gfp* cells transformed with a vector control or an *asp1*$^{365\text{-}920}$ expressing plasmid. Scale bar= 2 µm. **B:** Quantification of the fluorescence signal of Cut7-GFP on short spindles. For relative signal intensity at the spindle midzone compared to the spindle ends, the fluorescence signal at the midzone was normalized against the background (square 5 – square 6) and divided by the fluorescence intensity at spindle ends (square 1 – square 2 and square 3 – square 4). **C:** Diagrammatic representation of the ratios spindle midzone/spindle ends (control: n= 29; pasp1$^{365\text{-}920}$ n= 24; ***: P ≤ 0.001, t-test; significant outliers removed using Grubbs' test.). **D:** Diagrammatic representation of the frequency of spindle breaks in the indicated transformants (control: n= 30; pasp1$^{365\text{-}920}$ n= 29; ***: P ≤ 0.001, χ^2-test). **E:** Diagrammatic representation of the ratios spindle midzone/spindle ends (control: n= 30; pasp1$^{365\text{-}920}$ non-breaking n= 23; pasp1$^{365\text{-}920}$ breaking n= 17 (9 cells); ***: P ≤ 0.001, *: P ≤ 0.05, t-test). **F:** Diagrammatic representation of the ratios spindle midzone/spindle ends (*asp1*$^{+}$ *cut7-GFP*: n= 29; *asp1*^{D333A} *cut7-GFP*: n= 24; ***: P ≤ 0.001, t-test; significant outliers removed using Grubbs' test). Analysis was carried out at 33 °C.

Fig 5. *asp1*^{D333A} cell population contains polyploid cells.

A: Photomicrographs of a mitotic *asp1*^{D333A} *bub3Δ* cell expressing *sad1*$^{+}$*-mCherry* and cen1-GFP. Time between images: 1 min. Scale bar= 2 µm. 2/11 analyzed *asp1*^{D333A} *bub3Δ* double mutant cells showed this phenotype. **B:** FACS analysis of the indicated strains. Cells were gated for size revealing that cell populations with an *asp1*^{D333A} background were much more heterogenous than *asp1*$^{+}$ populations. The P2 area contains the largest cells. **C:** Measurement of DNA content (2-32N) of the

indicated cell population; left: entire population; right: P2 population. DNA content of peaks was defined by using the *cdc11-123* strain as standard (Suppl. Fig 5) (65).

Fig 6. Loss of functional Asp1 pyrophosphatase domain results in increased IP_8 levels.

A: Diagrammatic representation of Asp1 variants analyzed. All variants were expressed from the endogenous *asp1*$^+$ locus. **B** and **C:** HPLC elution profile of inositol polyphosphates of the wild-type type (WT) or *asp1*^{H397A} strain. **D:** Comparison of part of the inositol pyrophosphate profiles of the wild-type and *asp1*^{H397A} strains. **E:** Diagrammatic representation of IP_8 levels relative to IP_7. (WT: n= 4; *asp1*^{H397A} n= 3; *: $P \leq 0.05$, t-test). The fold-change of IP_8/ IP_7 is 2.81 higher for the *asp1*^{H397A} strain compared to the wild-type strain. **F:** HPLC elution profile of inositol polyphosphates of the *asp1*$^{1-364}$ strain. **G:** Comparison of inositol pyrophosphate profiles of the wild-type and *asp1*$^{1-364}$ strains (data used for this wild-type were obtained from a strain grown in parallel to the *asp1*$^{1-364}$ strain) and **H:** Diagrammatic representation of IP_8 levels relative to IP_7 and normalized to the wild-type. (WT: n= 4; Asp1$^{1-364}$ n= 3; **: $P \leq 0.01$, t-test). The fold-change of IP_8/ IP_7 is 1.67 higher for the *asp1*$^{1-364}$ strain compared to the wild-type strain.

Fig 7. The conserved amino acids of the M1 motif are essential for pyrophosphatase activity.

A: Diagrammatic representation of Asp1 pyrophosphatase M1 motif mutants. **B:** *In vitro* pyrophosphatase assay with using Asp1$^{365-920}$, Asp1$^{365-920/H397A}$, Asp1$^{365-920/R400A}$ or Asp1$^{365-920/R396A}$. 8 µg of the indicated proteins were added to Asp1 kinase

generated IP_7 (input shown in lane 1), incubated for 16 h and the resulting inositol polyphosphates resolved on a 35.5% PAGE and stained with Toluidine Blue; - component not added , + component added. All pyrophosphatase variants were tested at least twice in the *in vitro* assay. **C:** Serial dilution patch tests (10^4 to 10^1 cells) of a wild-type strain transformed with vector (control) or plasmids expressing the indicated *asp1* variants via the *nmt1*$^+$ promoter. Transformants were grown under plasmid selective conditions with or without thiamine and with or without 7 µg/ ml TBZ at 25°C for 7 days. **D:** Serial dilution patch tests (10^4 to 10^1cells) of an *asp1Δ* strain transformed with vector (control) or plasmids expressing *asp1*$^+$ or *asp1*^{R400A} from the *nmt1*$^+$ promoter. Transformants were grown as in C. **E:** Invasive growth assay. Left: 10^5 wild-type cells transformed with vector control, *asp1*$^+$, *asp1*^{H397A} or *asp1*^{R400A} plasmids were grown on plasmid selective thiamine-plus medium for 21 days at 30°C (top panels, surface growth). Removal of surface growth by washing revealed invasively growing colonies (bottom panels). **F:** Quantification of invasively growing colonies; per plasmid 3 transformants were analyzed in triplicate, ***$P < 0.0005$, t-test. Number of invasive colonies: 81± 6 for *asp1*^{H397A} and 113 ± 8 for *asp1*^{R400A}.

Fig 8. **The I808D mutation abolishes Asp1 pyrophosphatase activity**

A: Diagrammatic representation of M2 motif mutants. **B:** *In vitro* pyrophosphatase assay using 8 µg protein of the indicated Asp1 variants. Assay performed as in Fig. 7B. The pyrophosphatase variants were tested at least twice in the *in vitro* assay. **C:** Serial dilution patch tests (10^4 to 10^1 cells) of a wild-type strain transformed with vector (control) or plasmids expressing *asp1*$^{365-920}$ or *asp1*$^{365-920/I808D}$ via *nmt1*$^+$. Transformants were grown under plasmid selective conditions with or without thiamine and with or without 7 µg/ ml TBZ at 25°C for 7 days. **D:** Serial dilution patch

946 tests (10^4 to 10^1 cells) of wild-type, *asp1Δ*, *asp1*^{H397A} and *asp1*^{I808D} strains grown on
947 YE5S full media at 25°C for 5 days with or without 12 µg/ml TBZ. **E:** HPLC elution
948 profile of inositol polyphosphates of the *asp1*^{I808D} strain. **F:** Comparison of inositol
949 pyrophosphate profiles of wild-type and *asp1*^{I808D} strains. **G:** IP_8 levels relative to IP_7
950 and normalized to the wild-type from data shown in F. (WT: n= 4; Asp1^{I808D} n= 3; *: P
951 ≤ 0.05, t-test). The fold-change of IP_8/ IP_7 is 2 for the *asp1*^{I808D} strain compared to the
952 wild-type strain.

953

954 **Fig 9. Characterization of the Asp1 interaction partner Met10.**

955 **A:** Yeast-two-hybrid analysis of the interaction between Asp1 and Met10
956 (SPCC584.01c). *S. cerevisiae* strain AH109 was co-transformed with a plasmid
957 expressing *asp1*$^+$ fused to the *GAL4* binding domain (pGBKT7) and a plasmid
958 expressing *met10* variant (aa 544-1006) fused to the *GAL4* activation domain
959 (pGADT7). Cells were spotted on plasmid selective SD medium with or without
960 histidine and incubated for 5 days at 30°C. **B:** Growth of wild-type and *met10Δ*
961 strains on the indicated media: full media (YE5S), minimal media (MM), MM plus 330
962 µM cysteine (MM+Cys), MM plus 140 µM methionine (MM+Met) or MM plus cysteine
963 and methionine (MM+Cys+Met). **C:** Serial dilution patch tests (10^4 to 10^1 cells) of
964 a wild-type strain transformed with vector (control) or plasmids expressing *asp1*$^+$ or
965 *met10*$^+$ from the *nmt1*$^+$ promoter. Transformants were grown at 25°C for 8 days. **D:**
966 Serial dilution patch tests (10^4 to 10^1 cells) of transformed *asp1Δ* cells with vector
967 (control) or plasmids expressing *asp1*$^+$ or *met10*$^+$ via *nmt1*$^+$. Incubation at 25°C for 11
968 days. **E:** Far western analysis. Far left: Coomassie stained gel of 1 µg of the
969 indicated purified proteins. Left: Protein-protein interaction of GST-Met10 (blotted

970 protein; 138 kDa, arrow) and Asp1$^{365-920}$-His (probe protein). Detection of GST-Met10
971 via His antibody. Middle: Control; Asp1$^{365-920}$-His (blotted protein) and GST (probe
972 protein) using a GST antibody. Right: Protein-protein interaction of Asp1$^{365-920}$-His
973 (blotted protein; 65 kDa, arrow) and GST-Met10 (probe protein). Detection of Asp1^{365-}
974 ^{920}-His via GST antibody. 1 µg of protein was loaded on the gel in all cases.
975 Concentration of probe proteins: 10 µg/ ml.

976

977 Fig 10. The mitochondrial associated Met10 protein inhibits Asp1
978 pyrophosphatase activity *in vitro*.

979 **A:** Live cell imaging of Met10-GFP cells stained with Mitotracker. Shown are
980 maximum-intensity-projection images of interphase cells grown at 25°C. Bar, 10µm.
981 **B:** Top: Live cell imaging of the mitochondrial protein Cox4-RFP in *asp1*$^{+}$ or ***asp1Δ***
982 cells. Shown are maximum-intensity-projection images of interphase cells grown at
983 25°C. # normal and * abnormal mitochondrial distribution. Bar, 10 µm. Bottom:
984 quantification of mitochondrial distribution: *asp1*$^{+}$ strain, n = 143; *asp1*^{H397A} strain, n =
985 77; ***asp1Δ*** strain, n=44; P** < 0.01, P*** < 0.001 χ2 test). **C:** *In vitro* pyrophosphatase
986 assay: input controls (lanes 1 and 8), 4 µg GST-Asp1$^{365-920}$ (lane 2), 4 µg GST-
987 Asp1$^{365-920}$ plus 6 µg Met10 (lane 3). *In vitro* pyrophosphatase assay using 4 µg
988 Asp$^{365-920}$-His (lane 4) or 4 µg Asp$^{365-920}$-His plus 8 µg Met10 (lane 5). *In vitro*
989 pyrophosphatase assay using 2 µg Ddp1-GST (lane 6) or 2 µg Ddp1-GST plus 6 µg
990 Met10 (lane 7). Lane 9 shows addition of 2 µg GST. *In vitro* pyrophosphatase assay
991 using 6 µg GST-Met10 and 2 µg GST (lane 10). *In vitro* pyrophosphatase assays
992 involving Met10 protein were repeated 4 times. All assays were incubated for 16 h
993 and the resulting inositol polyphosphates resolved on a 35.5% PAGE and stained

994 with Toluidine Blue; - component not added , + component added. Size of proteins
995 used in C: GST-Asp1: ~91 kDa, GST-Met10: ~138 kDa, Asp1$^{365-920}$-His: ~66 kDa,
996 GST-Ddp1: ~48 kDa.

997

998 **Table 1. Strains used in this study.**

S.pombe	genotype	source
UFY605	*his3-D1, ade6-M210, leu1-32,ura4-D18, h$^-$*	K. Gould
UFY1156	*asp1Δ::kan^R, his3-D1, ade6-M216, leu1-32, ura4-D18, h$^-$*	U. Fleig
UFY1511	*asp1^{D333A}::kan^R, his3-D1, ade6-M210, leu1-32, ura4-D18, h$^+$*	U. Fleig
UFY1565	*cdc11-123, leu$^-$, h$^-$*	FY8347 (Yeast Genetic Research Center Osaka, Japan)
UFY1579	*asp1^{H397A}::kan^R, his3-D1, ade6-M210, leu1-32, ura4-D18, h$^+$*	U. Fleig
UFY1687	*cut7-GFP::kan^R, cut12-CFP::nat^R, leu1, ura4, h$^-$*	FY17673 (Yeast Genetic Research Center Osaka, Japan)
UFY2257	*bub3Δ::kan^R, leu1$^-$, h$^-$*	FY18583 (Yeast Genetic Research Center Osaka, Japan)
UFY2290	*bub3Δ::kan^R, asp1^{D333A}::kan^R*	U. Fleig
UFY2294	*asp1$^{1-364}$::kan^R, ura4-D18, leu1-32, his3-D1, ade6-M21x, h$^+$*	This study
UFY2386	*bub3Δ::kan^R, asp1^{D333A}::kan^R sad1-mCherry::kan^R, LacI-GFP::his7$^+$, LacO-repeat::lys1$^+$, lys1-131, his7-366, h$^-$*	U. Fleig
UFY2553	*asp1^{I808D}::kan^R, his3-D1, ade6-M210, leu1-32, ura4-D18, h$^-$*	This study

UFY2758	*met10Δ::kan^R, his3-D1, ade6-M210, leu1-32, ura4-D18, h$^-$*	This study
UFY2795	*met10-GFP::kan^R, his3-D1, ade6-M210, leu1-32, ura4-D18, h$^-$*	This study
UFY2805	*met10Δ::kan^R, asp1^{D333A}::kan^R, his3-D1, ade6-M210, leu1-32, ura4-D18, h$^-$*	This study
UFY2807	*met10Δ::kan^R, asp1^{H397A}::kan^R, his3-D1, ade6-M210, leu1-32, ura4-D18, h$^-$*	This study
UFY2860	*met10Δ::kan^R, mal3Δ::his3, ade6-M210, leu1-32, ura4-D18, his3-D, h$^+$*	This study
UFY2940	*asp1^{D333A}-GFP::ura4$^+$, cox4-RFP::LEU2, ade6-M210, leu1-32, ura4-D18, his3-D1, h$^-$*	This study
UFY2941	*asp1-pk-GFP::ura4$^+$, cox4-RFP::LEU2, ade6-M21x, leu1-32, ura4-D18, his3-D1, h$^+$*	This study
UFY2951	*asp1Δ::kan^R, cox4-RFP::LEU2 , ura4-D18, leu1-32, his3-D1, ade6-M21x, h$^-$*	This study
UFY3035	*cut7-GFP::kan^R, leu1, ura4, his3-D1*	This study
UFY3039	*asp1^{D333A}::kan^R, cut7-GFP::kan^R, his3-D1, ade6$^-$, leu1, ura4*	This study

S.cerevisiae	***genotype***	**source**
AH109	*MATa ura3-52, trp1-901, leu2-3,112, his3-200, gal4Δ, gal80Δ, LYS2::GAL1$_{UAS}$-GAL1$_{TATA}$-HIS3, GAL2$_{UAS}$-GAL2$_{TATA}$-ADE2, URA3::MEL1$_{UAS}$-MEL1$_{TATA}$-lacZ*	Clontech
Y187	*MATα ura3-52, trp1-901, leu2-3,112, his3-200, gal4Δ, met$^-$, gal80Δ, URA3:: GAL1$_{UAS}$-GAL1$_{TATA}$-lacZ*	Clontech
E. coli	***genotype***	**source**

	Rosetta (DE3)	*F^- ompT $hsdS_B(r_B^- m_B^-)$ gal dcm (DE3) pRARE (Cam^R)*	Novagen

999

1000

F1

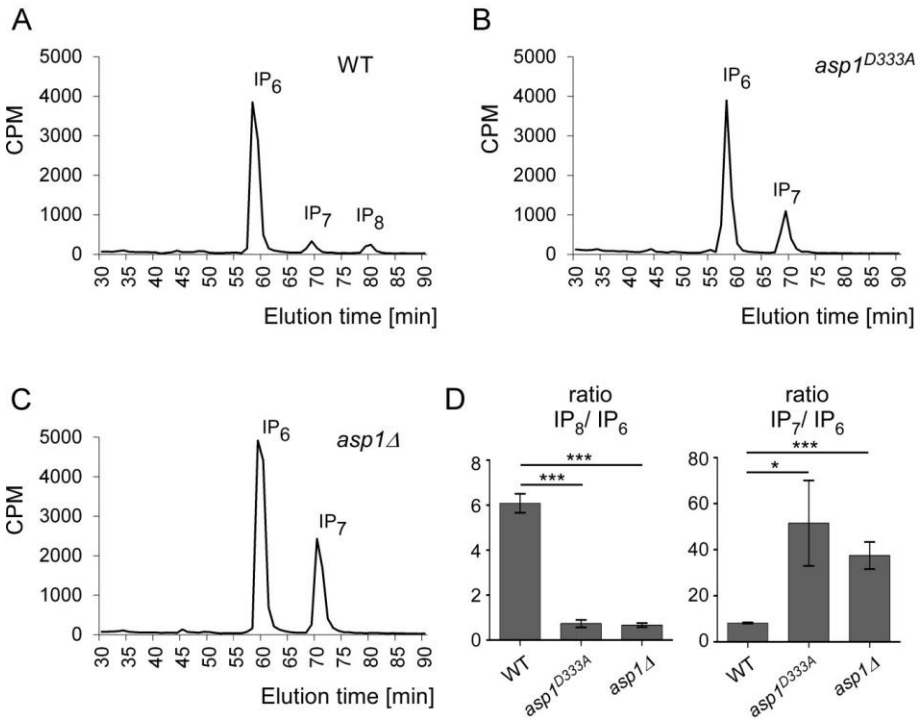

Fig 1. Asp1 kinase generates IP_8.

A to **C:** HPLC elution profiles of inositol polyphosphates of wild-type (WT), *asp1*^{D333A} and *asp1Δ* strains. *S. pombe* cells were radiolabeled with [^{3}H]inositol and cell lysates separated using anion-exchange HPLC. CPM: counts per minute. **D:** Left: diagrammatic representation of IP_8 levels relative to IP_6. Right: diagrammatic representation of IP_7 levels relative to IP_6. (WT: n= 3; *asp1*^{D333A} n= 2; ***asp1Δ*** n= 3. ***: $P \leq 0.001$; *: $P \leq 0.05$, t-test). The fold-change of IP_8/ IP_6 is as follows: (WT set at 1.00); 0.12 (*asp1*^{D333A}*)* and 0.11 *(asp1Δ).* Fold-change of IP_7/ IP_6: 6.26 (*asp1*^{D333A}*)* and 4.56 *(asp1Δ).*

F2

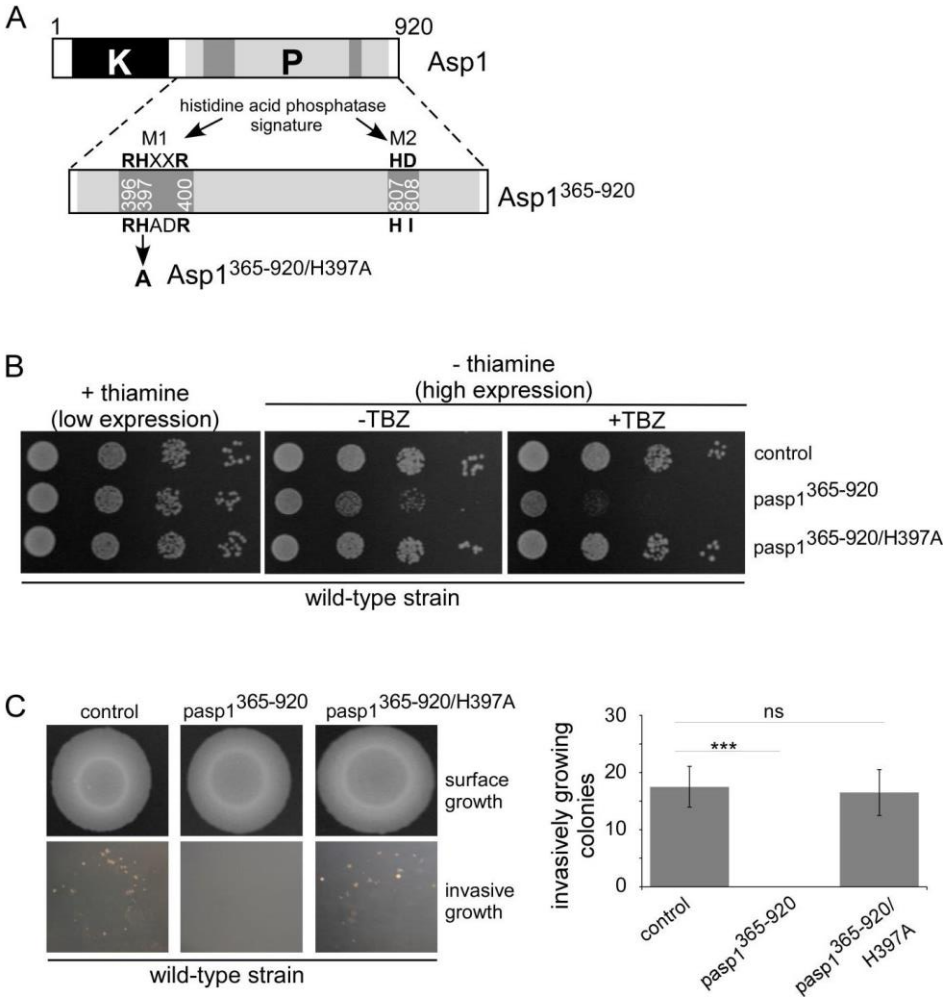
A
1
920
K
P
Asp1
histidine acid phosphatase signature
M1
RHXXR
M2
HD
396
397
400
307
308
Asp1365-920
RHADR
H I
A
Asp1365-920/H397A
B
+ thiamine (low expression)
- thiamine (high expression)
-TBZ
+TBZ
control
pasp1365-920
pasp1365-920/H397A
wild-type strain
C
control
pasp1365-920
pasp1365-920/H397A
surface growth
invasive growth
wild-type strain
invasively growing colonies
30
20
10
0
ns
***
control
pasp1365-920
pasp1365-920/ H397A

Fig 2. *In vivo* analysis of Asp1$^{365\text{-}920}$ and Asp1$^{365\text{-}920/H397A}$ function.

A: Diagrammatic representation of the dual-domain structure of Asp1 with kinase (K, black box) and pyrophosphatase (P, light grey box) regions. Enlargement of pyrophosphatase domain with the signature motifs M1 and M2 of histidine acid phosphatases (dark grey boxes) (1). In Asp1, the aspartate residue of M2 is replaced by isoleucine (H**I** instead of H**D**). **B:** Serial dilution patch tests (10^4 to 10^1 cells) of a wild-type strain transformed with vector (control) or plasmids expressing *asp1*$^{365–920}$ or *asp1*$^{365–920/H397A}$ from the thiamine-repressible promoter *nmt1*$^+$. Transformants were grown under plasmid selective conditions in absence or presence of 7 µg/ ml TBZ at 25°C for 7 days. **C:** Invasive growth assay. Left: A total of 10^5 wild-type cells transformed with either vector control or plasmids with *asp1*$^{365–920}$ or *asp1*$^{365-920/H397A}$ were spotted on plasmid selective medium without thiamine and incubated for 21 days at 30°C (top panels, surface growth). Plates were washed and all surface growth rubbed off. Invasively growing colonies remained (bottom panels) and were counted. Quantification shown on the right: 3 transformants were analyzed per plasmid in triplicate, ns= not significant, ***: $P < 0.0005$, t test. The number of agar-invading colonies of the *asp1*$^{365-920/H397A}$ transformants and the control transformants were 16.5± 4.0 and 17.5± 3.6, respectively.

F3

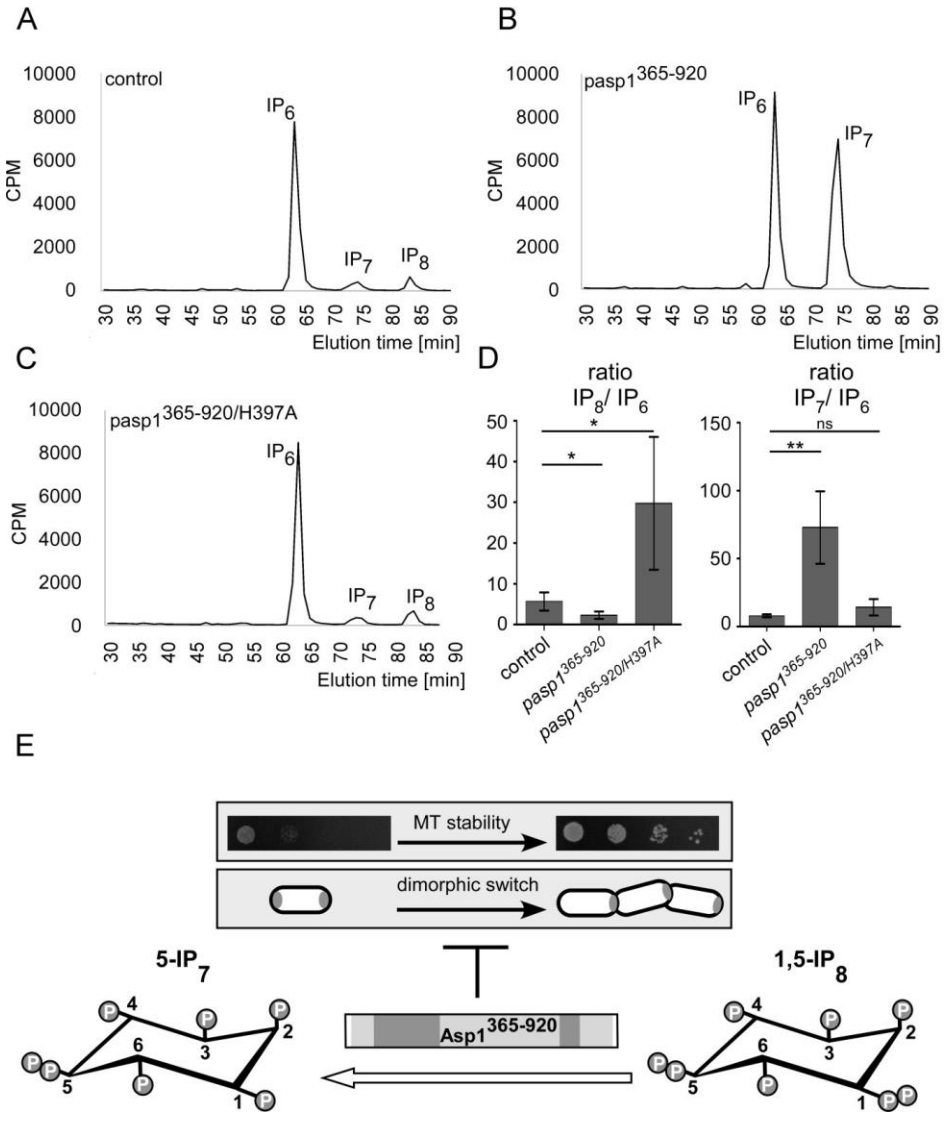
A
control
IP6
IP7
IP8
CPM
Elution time [min]
B
pasp1365-920
IP6
IP7
CPM
Elution time [min]
C
pasp1365-920/H397A
IP6
IP7
IP8
CPM
Elution time [min]
D
ratio IP8/ IP6
ratio IP7/ IP6
control
pasp1365-920
pasp1365-920/H397A
ns
E
MT stability
dimorphic switch
5-IP7
1,5-IP8
Asp1365-920

Fig 3. Asp1$^{365-920}$ has pyrophosphatase activity *in vivo.*

A to **C:** HPLC elution profiles of inositol polyphosphates of the wild-type strain transformed with (**A**) vector control or *asp1$^{365–920}$* or *asp1$^{365–920/H397A}$* expressing plasmids (**B** and **C**, respectively). Cells were radiolabeled with [^{3}H] inositol and cell lysates separated using anion-exchange HPLC. **D:** Diagrammatic representation of IP_8 levels relative to IP_6 (left) and IP_7 levels relative to IP_6 (right) normalized to the vector control using data from A, B and C**.** (control: n= 4; pasp1$^{365-920}$ n= 4; pasp1$^{365-920/H397A}$ n= 4. **: $P \leq 0.01$; *: $P \leq 0.05$; ns: not significant, t-test). The fold-change of IP_8/ IP_6 is as follows: (control set at 1.00); 0.4 (pasp1$^{365-920}$) and 5.3 (pasp1$^{365-920/H397A}$). Fold-change of IP_7/ IP_6: 9.3 (pasp1$^{365-920}$) and 1.8 (pasp1$^{365-920/H397A}$). **E:** MT stability and the dimorphic switch require intracellular IP_8, which are down-regulated by Asp1 pyrophosphatase activity.

F4

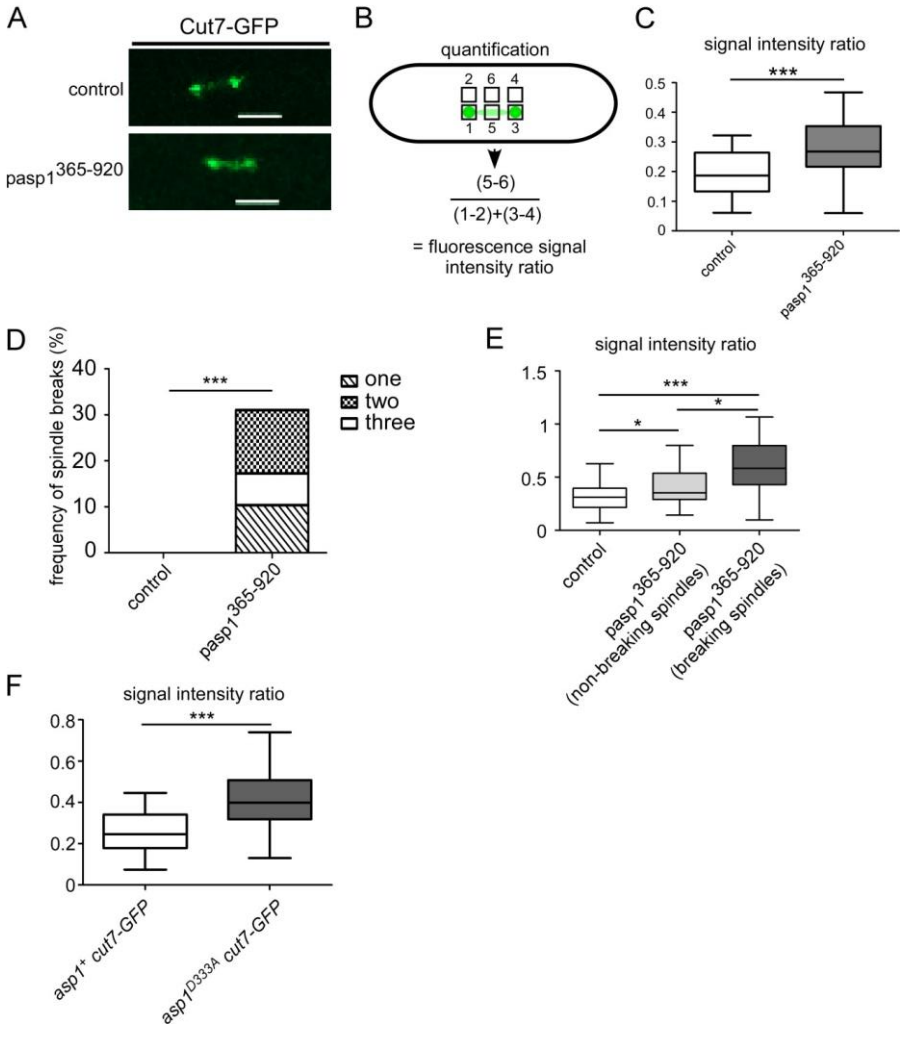
A
Cut7-GFP
control
pasp1365-920
B
quantification
2 6 4
1 5 3
(5-6)
(1-2)+(3-4)
= fluorescence signal intensity ratio
C
signal intensity ratio
***
0.5
0.4
0.3
0.2
0.1
0
control
pasp1365-920
D
frequency of spindle breaks (%)
40
30
20
10
0
***
one
two
three
control
pasp1365-920
E
signal intensity ratio
1.5
1
0.5
0
***
*
*
control
pasp1365-920 (non-breaking spindles)
pasp1365-920 (breaking spindles)
F
signal intensity ratio
0.8
0.6
0.4
0.2
0
***
asp1+ cut7-GFP
asp1D333A cut7-GFP

Fig 4. IP_8 controls Cut7-GFP spindle association.

A: Photomicrographs of *cut7*$^{+}$*-gfp* cells transformed with a vector control or an *asp1*$^{365\text{-}920}$ expressing plasmid. Scale bar= 2 μm. **B:** Quantification of the fluorescence signal of Cut7-GFP on short spindles. For relative signal intensity at the spindle midzone compared to the spindle ends, the fluorescence signal at the midzone was normalized against the background (square 5 – square 6) and divided by the fluorescence intensity at spindle ends (square 1 – square 2 and square 3 – square 4). **C:** Diagrammatic representation of the ratios spindle midzone/spindle ends (control: n= 29; pasp1$^{365\text{-}920}$ n= 24; ***: P ≤ 0.001, t-test; significant outliers removed using Grubbs' test.). **D:** Diagrammatic representation of the frequency of spindle breaks in the indicated transformants (control: n= 30; pasp1$^{365\text{-}920}$ n= 29; ***: P ≤ 0.001, χ^2-test). **E:** Diagrammatic representation of the ratios spindle midzone/spindle ends (control: n= 30; pasp1$^{365\text{-}920}$ non-breaking n= 23; pasp1$^{365\text{-}920}$ breaking n= 17 (9 cells); ***: P ≤ 0.001, *: P ≤ 0.05, t-test). **F:** Diagrammatic representation of the ratios spindle midzone/spindle ends (*asp1*$^{+}$ *cut7-GFP*: n= 29; *asp1*^{D333A} *cut7-GFP*: n= 24; ***: P ≤ 0.001, t-test; significant outliers removed using Grubbs' test). Analysis was carried out at 33 °C.

F5

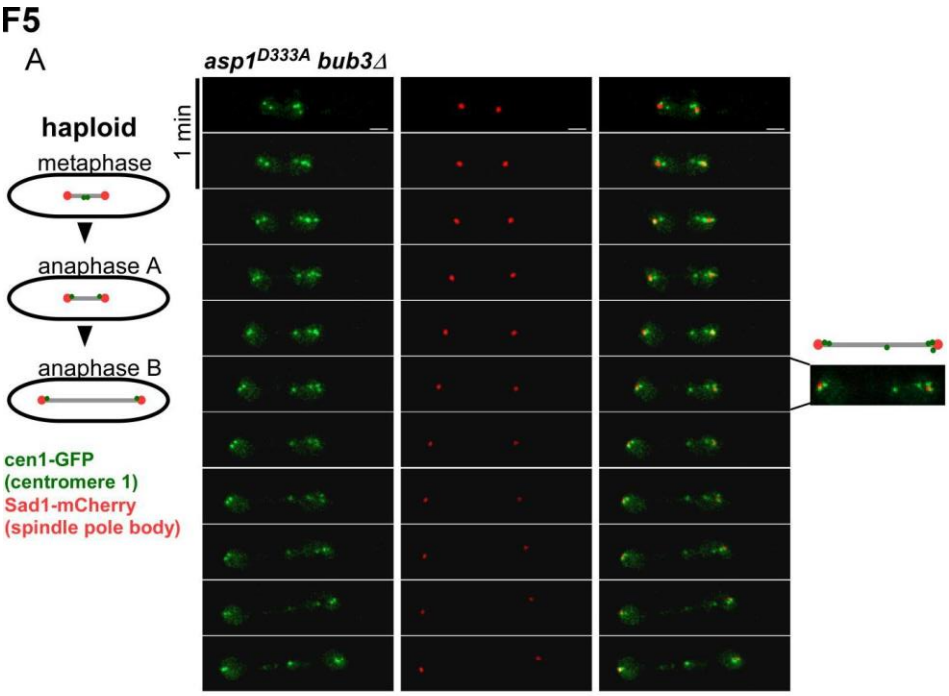
A
asp1D333A bub3Δ
haploid
metaphase
anaphase A
anaphase B
1 min
cen1-GFP
(centromere 1)
Sad1-mCherry
(spindle pole body)

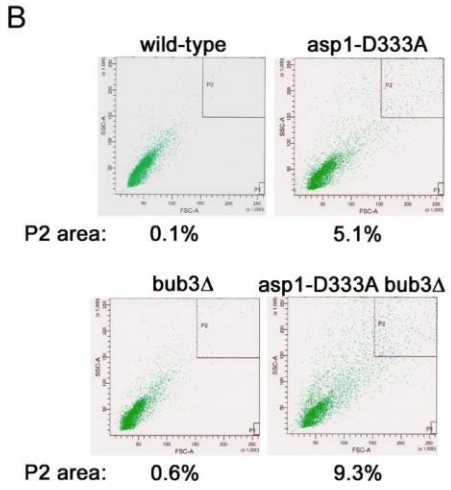
B
wild-type
asp1-D333A
P2 area: 0.1% 5.1%
bub3Δ
asp1-D333A bub3Δ
P2 area: 0.6% 9.3%

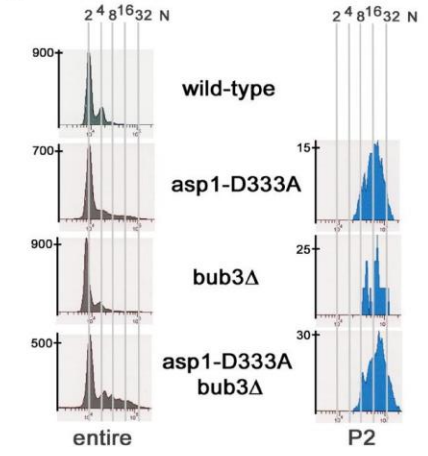
C
2 4 8 16 32 N
900
700
900
500
wild-type
asp1-D333A
bub3Δ
asp1-D333A bub3Δ
15
25
30
entire
P2

Fig 5. *asp1^{D333A}* cell population contains polyploid cells.

A: Photomicrographs of a mitotic *asp1^{D333A} bub3Δ* cell expressing *sad1^{+}-mCherry* and cen1-GFP. Time between images: 1 min. Scale bar= 2 μm. 2/11 analyzed *asp1^{D333A} bub3Δ* double mutant cells showed this phenotype. **B:** FACS analysis of the indicated strains. Cells were gated for size revealing that cell populations with an *asp1^{D333A}* background were much more heterogenous than *asp1^{+}* populations. The P2 area contains the largest cells. **C:** Measurement of DNA content (2-32N) of the indicated cell population; left: entire population; right: P2 population. DNA content of peaks was defined by using the *cdc11-123* strain as standard (Suppl. Fig 5) (65).

F6

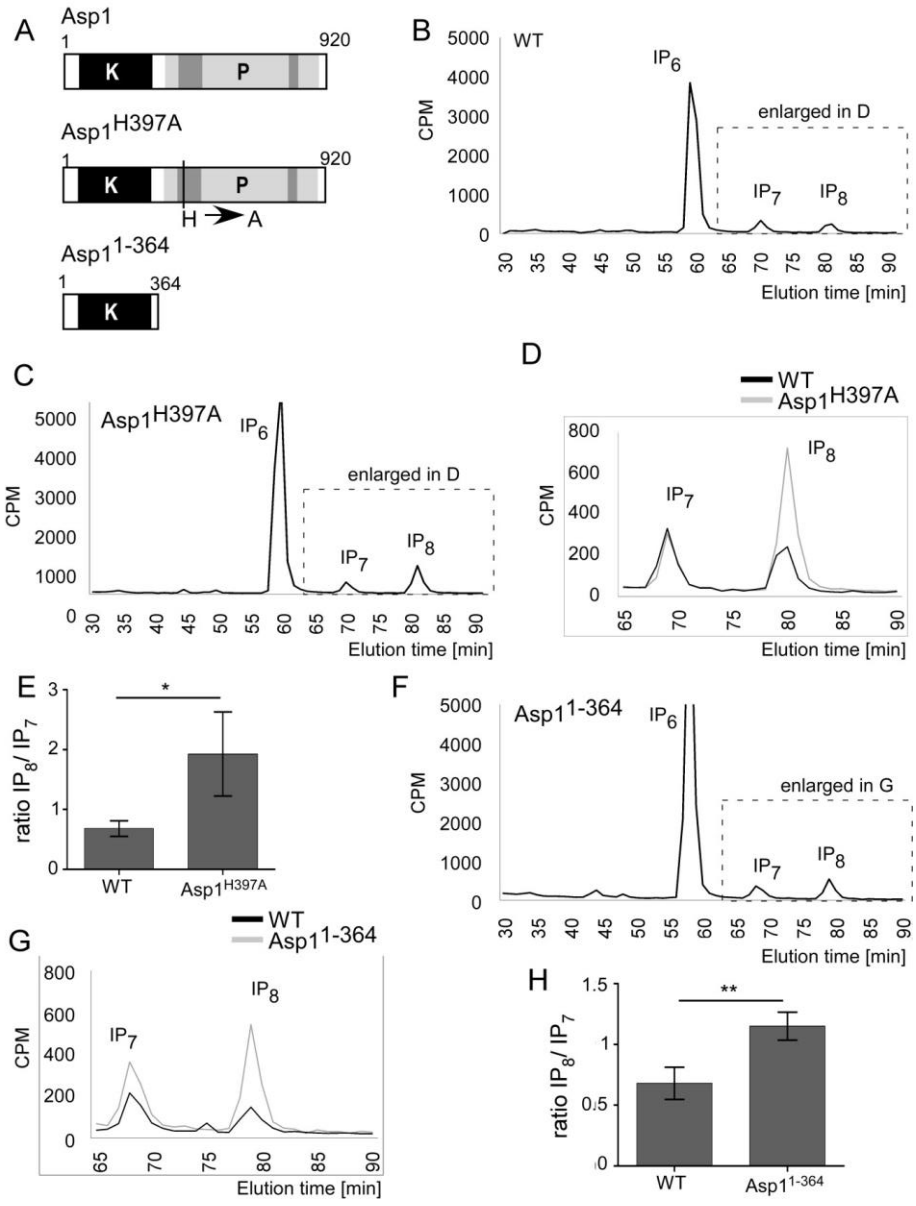
A
Asp1
1
920
K
P
Asp1H397A
H → A
Asp1 1-364
364
B
WT
IP6
enlarged in D
IP7
IP8
CPM
Elution time [min]
C
Asp1H397A
D
WT
Asp1H397A
E
ratio IP8/ IP7
*
F
Asp1 1-364
enlarged in G
G
H
**

Fig 6. Loss of functional Asp1 pyrophosphatase domain results in increased IP_8 levels.

A: Diagrammatic representation of Asp1 variants analyzed. All variants were expressed from the endogenous *asp1*$^{+}$ locus. **B** and **C:** HPLC elution profile of inositol polyphosphates of the wild-type type (WT) or *asp1*^{H397A} strain. **D:** Comparison of part of the inositol pyrophosphate profiles of the wild-type and *asp1*^{H397A} strains. **E:** Diagrammatic representation of IP_8 levels relative to IP_7. (WT: n= 4; *asp1*^{H397A} n= 3; *: $P \leq 0.05$, t-test). The fold-change of IP_8/ IP_7 is 2.81 higher for the *asp1*^{H397A} strain compared to the wild-type strain. **F:** HPLC elution profile of inositol polyphosphates of the *asp1*$^{1-364}$ strain. **G:** Comparison of inositol pyrophosphate profiles of the wild-type and *asp1*$^{1-364}$ strains (data used for this wild-type were obtained from a strain grown in parallel to the *asp1*$^{1-364}$ strain) and **H:** Diagrammatic representation of IP_8 levels relative to IP_7 and normalized to the wild-type. (WT: n= 4; Asp1$^{1-364}$ n= 3; **: $P \leq 0.01$, t-test). The fold-change of IP_8/ IP_7 is 1.67 higher for the *asp1*$^{1-364}$ strain compared to the wild-type strain.

F7

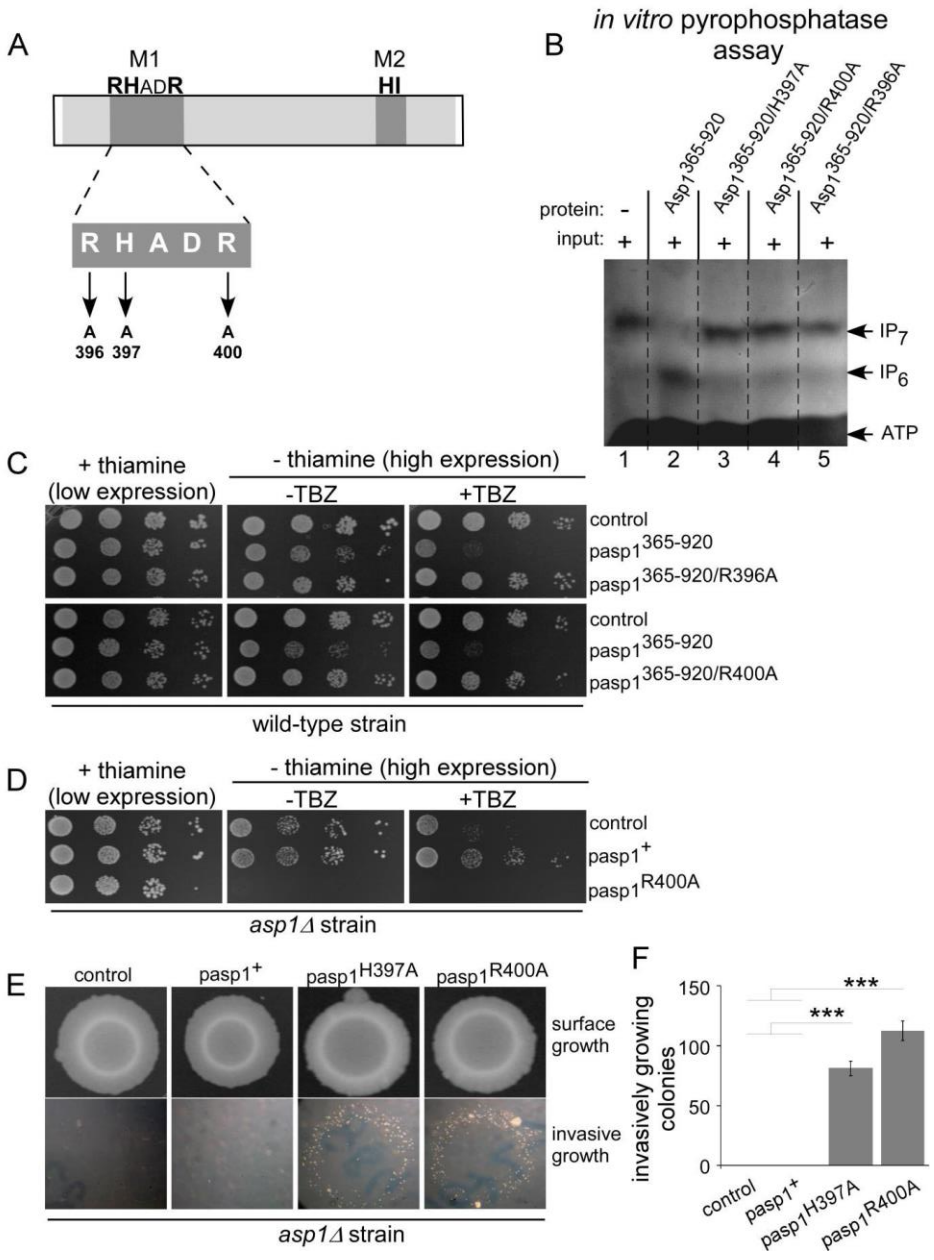
A
M1
RHADR
M2
HI
R H A D R
A 396
A 397
A 400
B
in vitro pyrophosphatase assay
Asp1365-920
Asp1365-920/H397A
Asp1365-920/R400A
Asp1365-920/R396A
protein: -
input: + + + + +
IP7
IP6
ATP
1 2 3 4 5
C
+ thiamine (low expression)
- thiamine (high expression)
-TBZ
+TBZ
control
pasp1365-920
pasp1365-920/R396A
control
pasp1365-920
pasp1365-920/R400A
wild-type strain
D
+ thiamine (low expression)
- thiamine (high expression)
-TBZ
+TBZ
control
pasp1+
pasp1R400A
asp1Δ strain
E
control
pasp1+
pasp1H397A
pasp1R400A
surface growth
invasive growth
asp1Δ strain
F
invasively growing colonies
150
100
50
0
***
***
control
pasp1+
pasp1H397A
pasp1R400A

Fig 7. The conserved amino acids of the M1 motif are essential for pyrophosphatase activity.

A: Diagrammatic representation of Asp1 pyrophosphatase M1 motif mutants. **B:** *In vitro* pyrophosphatase assay with using $Asp1^{365\text{-}920}$, $Asp1^{365\text{-}920/H397A}$, $Asp1^{365\text{-}920/R400A}$ or $Asp1^{365\text{-}920/R396A}$. 8 µg of the indicated proteins were added to Asp1 kinase generated IP_7 (input shown in lane 1), incubated for 16 h and the resulting inositol polyphosphates resolved on a 35.5% PAGE and stained with Toluidine Blue; - component not added , + component added. All pyrophosphatase variants were tested at least twice in the *in vitro* assay. **C:** Serial dilution patch tests (10^4 to 10^1 cells) of a wild-type strain transformed with vector (control) or plasmids expressing the indicated *asp1* variants via the *nmt1*$^+$ promoter. Transformants were grown under plasmid selective conditions with or without thiamine and with or without 7 µg/ ml TBZ at 25°C for 7 days. **D:** Serial dilution patch tests (10^4 to 10^1cells) of an ***asp1Δ*** strain transformed with vector (control) or plasmids expressing *asp1*$^+$ or $asp1^{R400A}$ from the *nmt1*$^+$ promoter. Transformants were grown as in C. **E:** Invasive growth assay. Left: 10^5 wild-type cells transformed with vector control, *asp1*$^+$, $asp1^{H397A}$ or $asp1^{R400A}$ plasmids were grown on plasmid selective thiamine-plus medium for 21 days at 30°C (top panels, surface growth). Removal of surface growth by washing revealed invasively growing colonies (bottom panels). **F:** Quantification of invasively growing colonies; per plasmid 3 transformants were analyzed in triplicate, ***$P < 0.0005$, t-test. Number of invasive colonies: 81± 6 for $asp1^{H397A}$ and 113 ± 8 for $asp1^{R400A}$.

F8

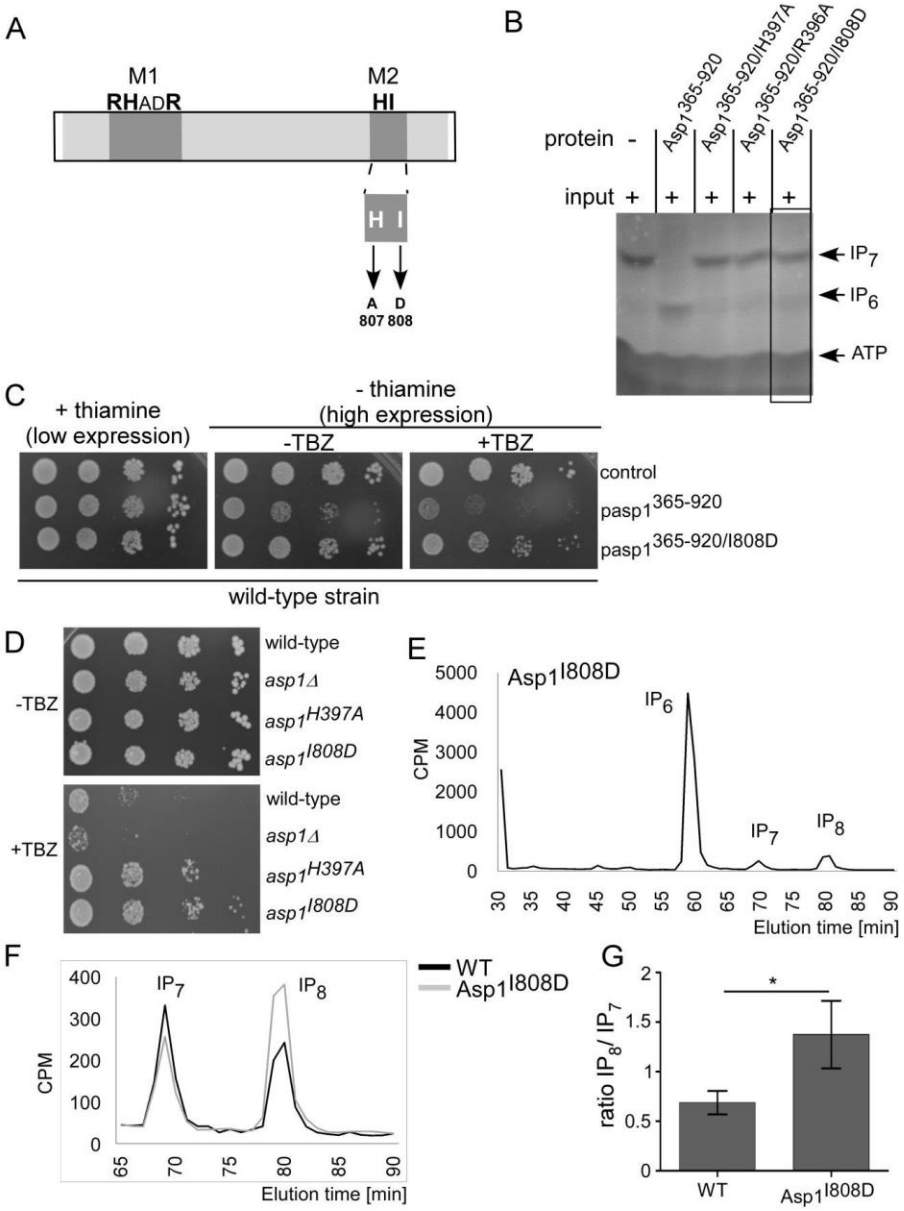
A
M1
RHADR
M2
HI
H I
A D
807 808
B
protein -
input +
Asp1365-920
Asp1365-920/H397A
Asp1365-920/R396A
Asp1365-920/I808D
IP7
IP6
ATP
C
+ thiamine
(low expression)
- thiamine
(high expression)
-TBZ
+TBZ
control
pasp1365-920
pasp1365-920/I808D
wild-type strain
D
-TBZ
+TBZ
wild-type
asp1Δ
asp1H397A
asp1I808D
E
Asp1I808D
IP6
IP7
IP8
CPM
Elution time [min]
F
IP7
IP8
WT
Asp1I808D
CPM
Elution time [min]
G
ratio IP8/ IP7
WT
Asp1I808D
*

Fig 8. **The I808D mutation abolishes Asp1 pyrophosphatase activity**

A: Diagrammatic representation of M2 motif mutants. **B:** *In vitro* pyrophosphatase assay using 8 μg protein of the indicated Asp1 variants. Assay performed as in Fig. 7B. The pyrophosphatase variants were tested at least twice in the *in vitro* assay. **C:** Serial dilution patch tests (10^4 to 10^1 cells) of a wild-type strain transformed with vector (control) or plasmids expressing *asp1*$^{365\text{-}920}$ or *asp1*$^{365\text{-}920/I808D}$ via *nmt1*$^+$. Transformants were grown under plasmid selective conditions with or without thiamine and with or without 7 μg/ ml TBZ at 25°C for 7 days. **D:** Serial dilution patch tests (10^4 to 10^1 cells) of wild-type, ***asp1Δ***, *asp1*^{H397A} and *asp1*^{I808D} strains grown on YE5S full media at 25°C for 5 days with or without 12 μg/ml TBZ. **E:** HPLC elution profile of inositol polyphosphates of the *asp1*^{I808D} strain. **F:** Comparison of inositol pyrophosphate profiles of wild-type and *asp1*^{I808D} strains. **G:** IP_8 levels relative to IP_7 and normalized to the wild-type from data shown in F. (WT: n= 4; Asp1^{I808D} n= 3; *: $P \leq 0.05$, t-test). The fold-change of IP_8/ IP_7 is 2 for the *asp1*^{I808D} strain compared to the wild-type strain.

F9

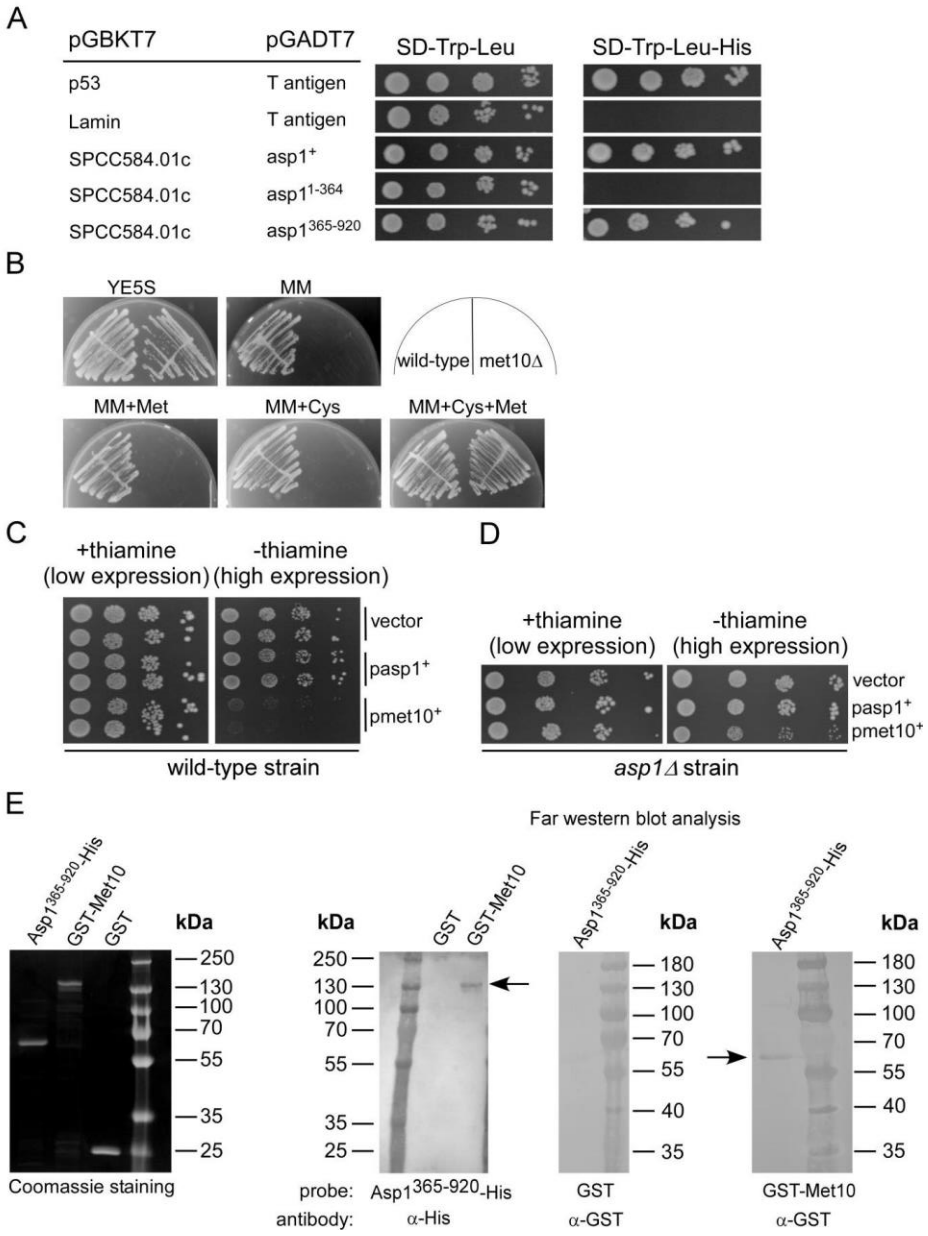
A
pGBKT7
pGADT7
SD-Trp-Leu
SD-Trp-Leu-His
p53
T antigen
Lamin
T antigen
SPCC584.01c
asp1+
SPCC584.01c
asp1 1-364
SPCC584.01c
asp1 365-920
B
YE5S
MM
wild-type
met10Δ
MM+Met
MM+Cys
MM+Cys+Met
C
+thiamine (low expression)
-thiamine (high expression)
vector
pasp1+
pmet10+
wild-type strain
D
+thiamine (low expression)
-thiamine (high expression)
vector
pasp1+
pmet10+
asp1Δ strain
E
Far western blot analysis
Asp1 365-920-His
GST-Met10
GST
kDa
250
130
100
70
55
35
25
Coomassie staining
probe: Asp1 365-920-His
antibody: α-His
GST
α-GST
GST-Met10
α-GST
180
40

Fig 9. Characterization of the Asp1 interaction partner Met10.

A: Yeast-two-hybrid analysis of the interaction between Asp1 and Met10 (SPCC584.01c). *S. cerevisiae* strain AH109 was co-transformed with a plasmid expressing *asp1*$^{+}$ fused to the *GAL4* binding domain (pGBKT7) and a plasmid expressing *met10* variant (aa 544-1006) fused to the *GAL4* activation domain (pGADT7). Cells were spotted on plasmid selective SD medium with or without histidine and incubated for 5 days at 30°C. **B:** Growth of wild-type and *met10Δ* strains on the indicated media: full media (YE5S), minimal media (MM), MM plus 330 µM cysteine (MM+Cys), MM plus 140 µM methionine (MM+Met) or MM plus cysteine and methionine (MM+Cys+Met). **C:** Serial dilution patch tests (10^4 to 10^1 cells) of a wild-type strain transformed with vector (control) or plasmids expressing *asp1*$^{+}$ or *met10*$^{+}$ from the *nmt1*$^{+}$ promoter. Transformants were grown at 25°C for 8 days. **D:** Serial dilution patch tests (10^4 to 10^1 cells) of transformed *asp1Δ* cells with vector (control) or plasmids expressing *asp1*$^{+}$ or *met10*$^{+}$ via *nmt1*$^{+}$. Incubation at 25°C for 11 days. **E:** Far western analysis. Far left: Coomassie stained gel of 1 µg of the indicated purified proteins. Left: Protein-protein interaction of GST-Met10 (blotted protein; 138 kDa, arrow) and Asp1$^{365\text{-}920}$-His (probe protein). Detection of GST-Met10 via His antibody. Middle: Control; Asp1$^{365\text{-}920}$-His (blotted protein) and GST (probe protein) using a GST antibody. Right: Protein-protein interaction of Asp1$^{365\text{-}920}$-His (blotted protein; 65 kDa, arrow) and GST-Met10 (probe protein). Detection of Asp1$^{365\text{-}920}$-His via GST antibody. 1 µg of protein was loaded on the gel in all cases. Concentration of probe proteins: 10 µg/ ml.

F10

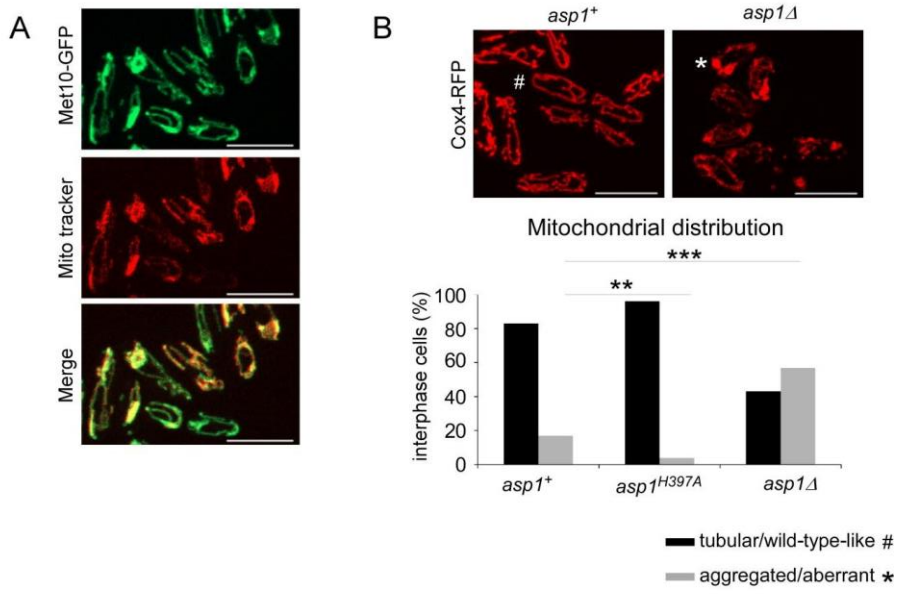

C

in vitro pyrophosphatase assay

1	2	3	4	5	6	7	8	9	10	
-	-	-	-	-	-	-	-	+	+	:GST
-	-	-	-	-	+	+	-	-	-	:Ddp1
-	-	+	-	+	-	+	-	-	+	:Met10
-	-	-	+	+	-	-	-	-	-	:Asp1$^{365-920}$-His
-	+	+	-	-	-	-	-	-	-	:GST-Asp1$^{365-920}$
+	+	+	+	+	+	+	+	+	+	:input

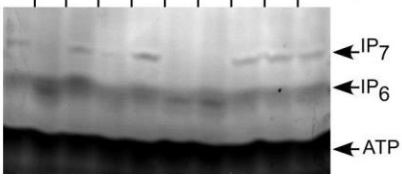

Fig 10. The mitochondrial associated Met10 protein inhibits Asp1 pyrophosphatase activity *in vitro*.

A: Live cell imaging of Met10-GFP cells stained with Mitotracker. Shown are maximum-intensity-projection images of interphase cells grown at 25°C. Bar, 10 μm. **B:** Top: Live cell imaging of the mitochondrial protein Cox4-RFP in *asp1*$^{+}$ or *asp1Δ* cells. Shown are maximum-intensity-projection images of interphase cells grown at 25°C. # normal and * abnormal mitochondrial distribution. Bar, 10 μm. Bottom: quantification of mitochondrial distribution: *asp1*$^{+}$ strain, n = 143; *asp1*^{H397A} strain, n = 77; *asp1Δ* strain, n=44; P** < 0.01, P*** < 0.001 $\chi 2$ test). **C:** *In vitro* pyrophosphatase assay: input controls (lanes 1 and 8), 4 μg GST-Asp1$^{365-920}$ (lane 2), 4 μg GST-Asp1$^{365-920}$ plus 6 μg Met10 (lane 3). *In vitro* pyrophosphatase assay using 4 μg Asp$^{365-920}$-His (lane 4) or 4 μg Asp$^{365-920}$-His plus 8 μg Met10 (lane 5). *In vitro* pyrophosphatase assay using 2 μg Ddp1-GST (lane 6) or 2 μg Ddp1-GST plus 6 μg Met10 (lane 7). Lane 9 shows addition of 2 μg GST. *In vitro* pyrophosphatase assay using 6 μg GST-Met10 and 2 μg GST (lane 10). *In vitro* pyrophosphatase assays involving Met10 protein were repeated 4 times. All assays were incubated for 16 h and the resulting inositol polyphosphates resolved on a 35.5% PAGE and stained with Toluidine Blue; - component not added , + component added. Size of proteins used in C: GST-Asp1: ~91 kDa, GST-Met10: ~138 kDa, Asp1$^{365-920}$-His: ~66 kDa, GST-Ddp1: ~48 kDa.